Beam optical calculations for SPIRAL2

R. Cee

Beam Optical Calculations for SPIRAL 2

Rainer Cee

GANIL R 04 01

Table of Content

Preface: Description of the SPIRAL 2 facility

SPIRAL 2 is the future facility for the production and acceleration of radioactive ion beams planed at GANIL, the large national heavy ion accelerator in Caen, France [1]. As of January 2004 the layout of SPIRAL 2 has the following appearance (see **Figure 1**): Two ion sources of ECR type for the production of deuterons respectively heavy ions with a mass-to-charge ratio A/q = 3 are installed on the ground floor which covers an area of 42×95 m². With an extraction voltage of typically 20-60 kV the beam is extracted from the source and injected into a four vane radio frequency quadrupole (RFQ), operated at 88 MHz, where the beam is pre-accelerated and bunched. An additional injector for the acceleration of ions with a mass-to-charge ratio A/q = 6, displayed in **Figure 1** as dashed red lines, is foreseen as option. With an energy gain of 750 keV/u the ions leave the RFQ and are further accelerated in the 88 MHz superconducting linac which is set up from two families of quarter-wave resonators designed for a velocity of β = 0.07 respectively β = 0.12. From here the primary beam with an energy of 40 MeV for deuterons and 14.5 MeV/u for ions is either transported directly into the stable ion experiment cave or downwards to the target-source assembly. Here, the deuteron is broken up in a carbon converter and a neutron induced nuclear fission takes place in a $^{238}UC_x$ target. After the ionisation in the 1+ ion source the radioactive secondary beam is mass separated and either guided to the low energy experimental hall, to an optional ion trap which might serve for an accumulation of the radioactive ions or via the charge breeder to the post accelerator CIME which is part of the existing SPIRAL facility. A mass identification subsequent to the mass separator outside the confinement area permits the determination of the beam purity. The radioactive ions might be transported to this identification station either by means of a beam line or a shuttle system.

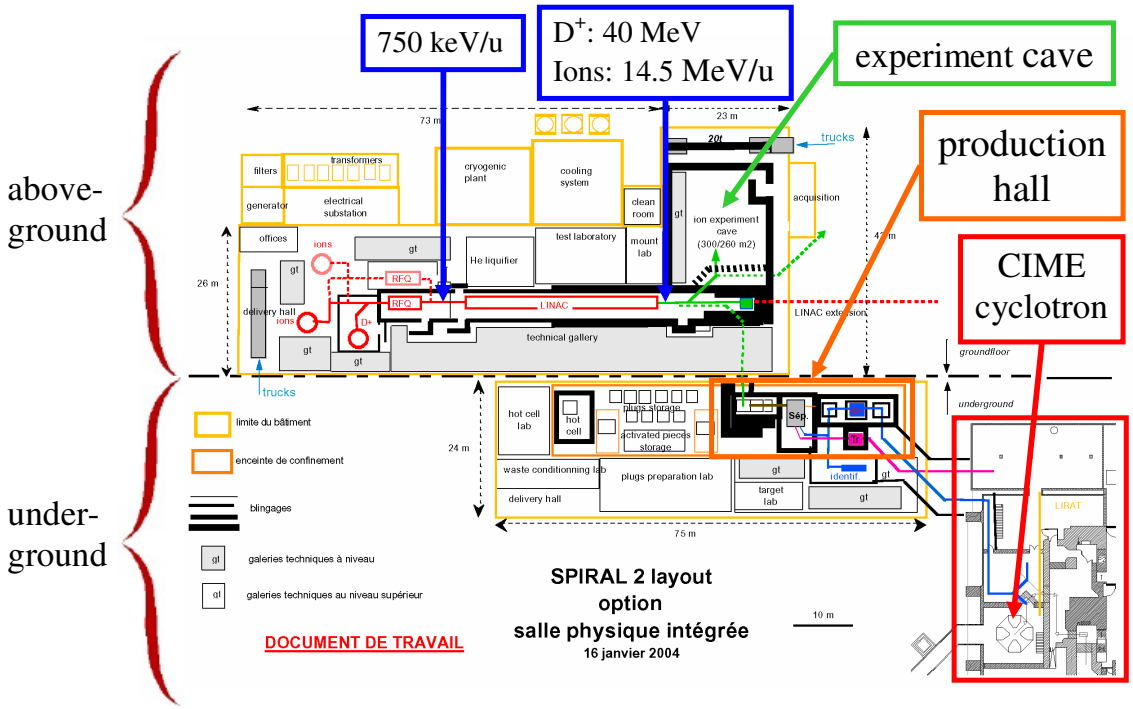

Figure 1: Layout of the SPIRAL 2 facility. Top: floor plan of the ground floor. Bottom: floor plan of the underground level. The lower right region marked by the red rectangular belongs to the already existing SPIRAL facility.

Part 1: Mass separation of the radioactive beam fragments

The radioactive fragments produced by the neutron induced fission of a ^{238}U target are distributed over a mass ranging from approximately A = 70 to A = 170. These isotopes diffuse from the target which is heated up to 2200°C into an ion source for 1+ ionisation. Several ion sources are in discussion (see **Table 1**) exhibiting different properties of the extracted beam. In terms of beam dynamics the most challenging ion source is the MONO1000 ECR source developed at GANIL with an rms-emittance of 70 π·mm·mrad. It is hence used as reference for the simulations in the frame of this work.

Table 1: Expected beam properties obtained with different types of 1+ ion sources [1].

Type of Ion Source	Emittance / π·mm·mrad	Diameter of Extraction Hole / mm	Origin of Data (U_{ext} = 34 kV)
ECR[1]	~70	4.0	MONO1000 (GANIL)
FEBIAD[2]	~30	1.6	ISOLDE
Surface	~15	3.0	IPNO & CSNSM, ISOLDE
Laser	~15	3.0	Estimation

The purpose of the mass separator is to filter out the desired charge state(s) from the "mass cocktail" delivered by the ion source by means of a dedicated mass spectrometer. The design goal is a mass resolution of R_m = 250 [1] (see Appendix 9.1 for definitions).

1 Status of the intermediate SPIRAL 2 report from December 2003

The mass separator should select and deliver at least two beams in the mass range from ~70 to ~170 simultaneously. To achieve this goal two different solutions for a mass separator have been proposed in the intermediate report of the SPIRAL 2 project published in December 2003 [1]. These two solutions are:

- A BRAMA solution, studied by IReS[3], based on sliding electrostatic deflectors which can deliver any mass to any channel.
- A fully magnetic separator (bi-selective solution), studied by GANIL (B. Bru, M. Duval), which is completely static and uses a dipole matrix to switch the required mass to the desired channel.

The principal element common to both solutions is an ELBEK spectrometer, a magnetic dipole which widely spreads the masses along a focal line [2]. It is a 104°

[1] **E**lectron **C**yclotron **R**esonance
[2] **F**orced **E**lectron **B**eam **I**on **A**rc **D**ischarge
[3] Institut de Recherches Subatomiques Strasbourg

bending device with rotated pole faces (see **Table 2** for characteristics). In **Figure 2** a TOSCA model of one pole, regarded from the inside, including yoke and coil is shown. In this illustration the beam enters the magnet from below and is bent to the right. The weight of the magnet amounts to 20.5 t where the main contribution (20 t) originates from the ion yoke, whereas the remainder is coming from the copper coil.

Table 2: Main geometrical characteristics of the ELBEK magnetic spectrometer [2].

PARAMETER	VALUE
sector angle	104°
entrance angle	45°
exit angle	-38°
object focal distance	1 m
image focal length	0.492 m (A = 70) to 0.812 m (A = 160)
curvature radii	0.836 m (A = 70) to 1.165 m (A = 160)
gap chamber	100 mm
magnet weight	20 t (iron) and 0.5 t (copper)
maximum induction	5 000 Gauß (0.5 T)

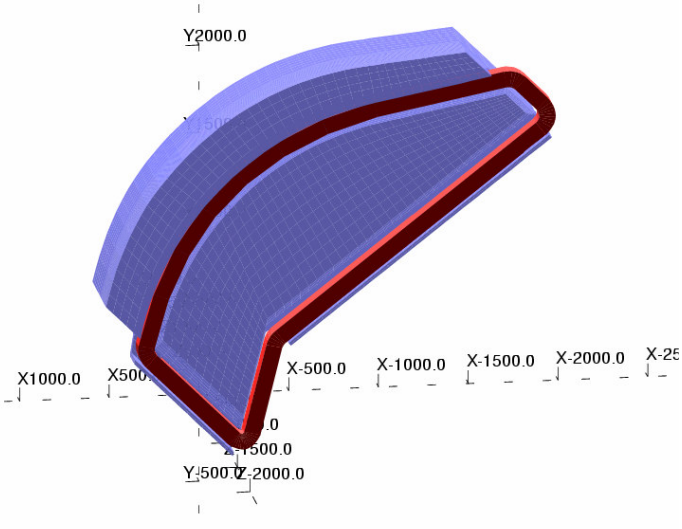

Figure 2: TOSCA 3D model of the ELBEK magnet (blue: yoke; red: copper coil). The beam enters the spectrometer from below and leaves it to the right after a deflection of 104°.

1.1 The BRAMA solution

In the BRAMA[4] solution the ELBEK magnet is followed by two electrostatic deflectors (**Figure 3**) [3]. These deflectors have a toroidal shape and act hence focusing in both transverse directions. The voltages applied are approximately one half of the extraction voltages. By moving the deflectors parallel to the focal line it is possible to switch any mass of the spectrum to one of the two channels and any other mass to the second one. The beam optics reveals the philosophy of the setup (**Figure 4**): the entrance wedge of the ELBEK magnet is horizontally defocusing and vertically focusing whereas the exit wedge has an opposite influence. The following deflector has a double focusing impact and the final waist is achieved by an electrostatic quadrupole doublet.

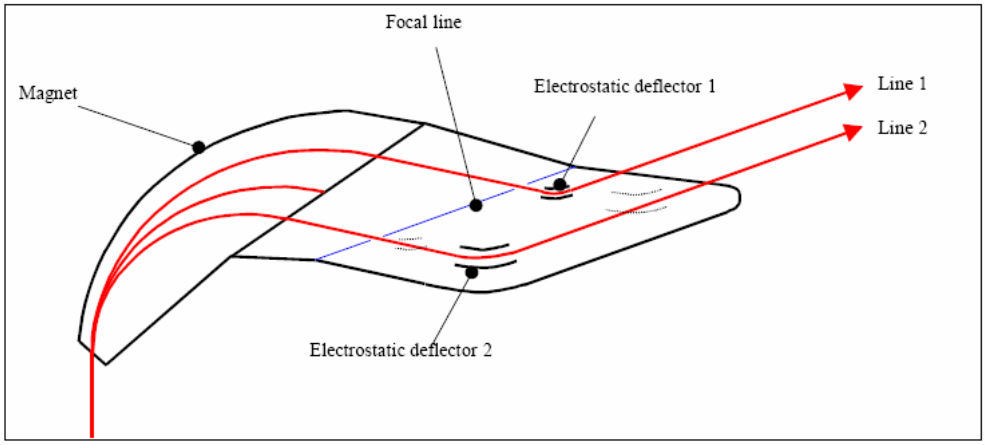

Figure 3: BRAMA solution with the ELBEK magnet and two electrostatic deflector movable along the focal line.

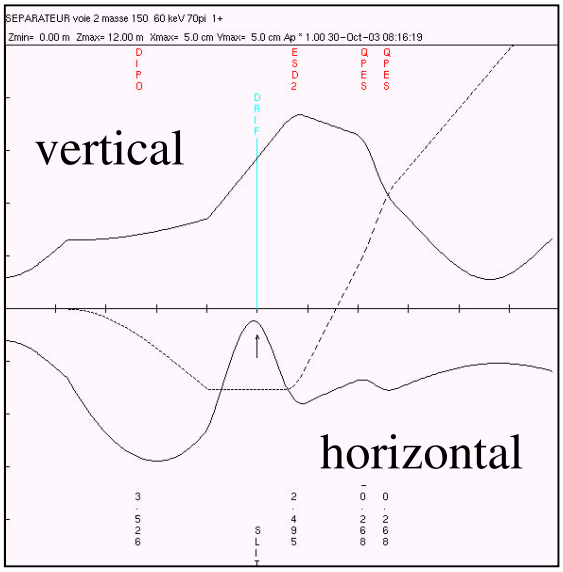

Figure 4: Beam optics of the BRAMA solution.

[4] **B**road **R**ange **A**tomic **M**ass **A**nalyser

1.2 The bi-selective solution

The bi-selective solution applies magnets instead of the electrostatic deflectors to bend the beams. Each channel consists of a small septum magnet and a larger analyser magnet. The analyser magnets of the two channels are identical whereas the septum magnets are individually designed. In principle each mass of the spectrum behind the ELBEK magnet enters one of the two beam lines. The beam optics of the upper beam line shows that the septum magnet has vertical focusing entrance and exit angle whereas the analyser magnet is the horizontally focusing at its entrance and vertically focusing at the exit.

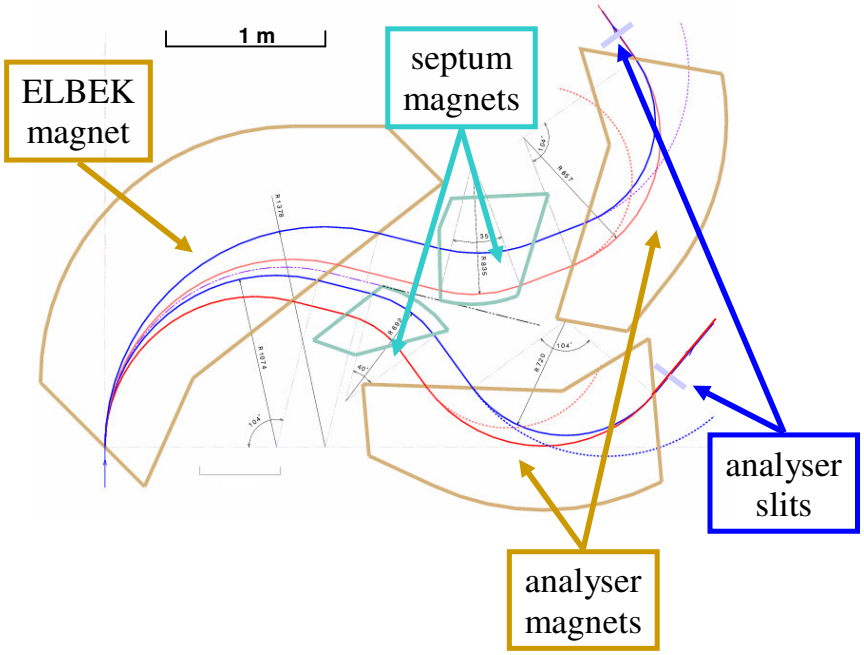

Figure 5: Bi-selective solution. The beam separation is achieved with magnetic devices solely.

The presented solutions for the mass separator exhibit several advantages but they also show some weak points. The ELBEK magnet itself provides a good resolution but has large dimensions. The optical focus in front of the magnet is another drawback regarding space charge effects of the beam not yet separated. The BRAMA solution is compact but contains complex, moving parts. Except for that, the electrostatic elements bear the risk of flashovers in a highly activated, ionised environment. In comparison to this the bi-selective solution is a relatively large device but it is mechanically static and has no electrostatic elements incorporated. To switch the two selected masses into the final beam lines an additional matrix of four magnets, not displayed in **Figure 5**, is required which even increases the total size of the setup. As we can see from this discussion it is worth thinking of alternatives as the solutions described above reveal some intrinsic drawbacks.

2 The Wien filter solution

As the radioactive ions extracted with the voltage U_{ext} from the $Q = 1$ e source have all the same kinetic energy $E_{kin} = ½ \cdot mv^2 = Q \cdot U_{ext}$ but different masses m they consequently differ in their velocity v. A device capable to separate velocities and in our case masses is the Wien velocity filter. Wien filters are commonly used to provide experimental beams of particles produced in accelerators. This principle is e.g. applied with great success at the LISE spectrometer for beam purification. Several setups for the SPIRAL 2 mass separator with a Wien filter as basic element have been investigated in this work and are described in the following preceded by a general section about the mode of operation of Wien filters and an introduction into the applied simulation programme COSY INFINITY.

2.1 Introduction

A good description of the functionality of a Wien filter can be found in [4]. More details of theoretical aspects can be obtained from [5]. Here only a summary is given.

2.1.1 The Wien velocity filter

A Wien filter basically consists of crosswise superposed static magnetic and electric fields which are oriented orthogonal to the direction of the beam. The transverse force F_x experienced by a particle with charge q and longitudinal velocity v_z when traversing a horizontal electric field E_x crossed with a vertical magnetic field B_y is given by

$$F_x = q\left(E_x - v_z \cdot B_y\right).$$

The force on a particle and hence the deviation vanishes if the so-called *straight-through condition*

$$v_z = \frac{E_x}{B_y}$$

is fulfilled.

In a velocity mixed beam all particles not accomplishing this condition are horizontally deflected either to the negative direction, if $v > v_z$, or to the positive direction, if $v < v_z$. By placing a vertical slit behind the filter, particles with the desired velocity can be separated from the others which are absorbed on the plates. When the particles have all the same mass the Wien filter acts also as energy filter. If the particles have all the same kinetic energy it can serve as mass filter. This is the case of the application at SPIRAL 2.

For the realisation of a Wien filter several design aspects have to be considered:

1. The electrodes and the magnet should generate electric and magnetic fields with the same fringe field distribution to guarantee the validity of the straight-through condition not only in the plateau region but throughout the structure.
2. As the Wien filter contains a magnetic field, it is astigmatic, i.e. there is a weak focusing in the plane of separation but no focusing effect in the perpendicular plane. This astigmatism can be corrected by means of a small quadrupole field within the filter. An electrode geometry and potential distribution as shown in **Figure 6** might serve for this purpose. Alternatively the astigmatism can be rectified by an external quadrupole.

3. Like every element containing electrostatic fields the Wien filter has aberrations, i.e. particles which are deflected gain or loose energy from the electrostatic field. This effect is compensated by the fringe fields in the outside region but has an effect on the beam optics inside the filter and should be minimised by choosing an appropriate length and field strengths.

Amongst these, the first item is the most crucial one. The resolution of the filter strongly depends on the fringe field shape. The ratio of electric to magnetic field should remain constant along the axis. This is generally difficult to fulfil in the fringe fields region as can be seen from **Figure 7** where the fringe field region of the LISE Wien filter exit is plotted.

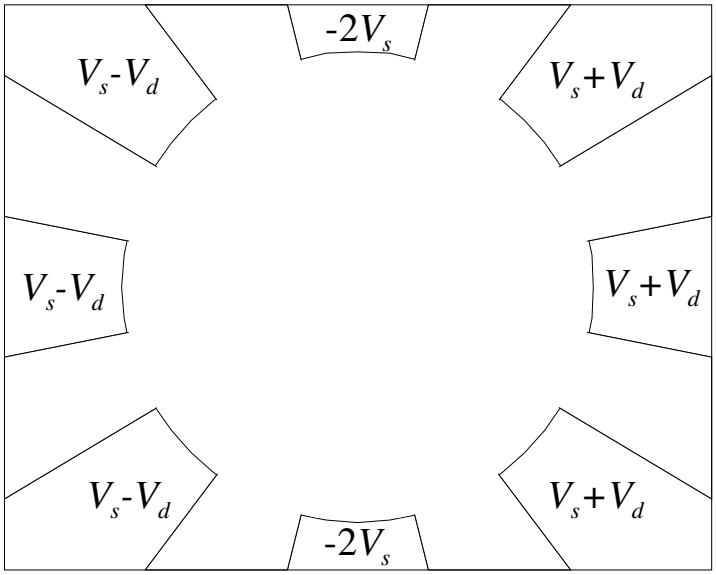

Figure 6: Electrode geometry and potential distribution to produce a combined dipole and quadrupole field [4].

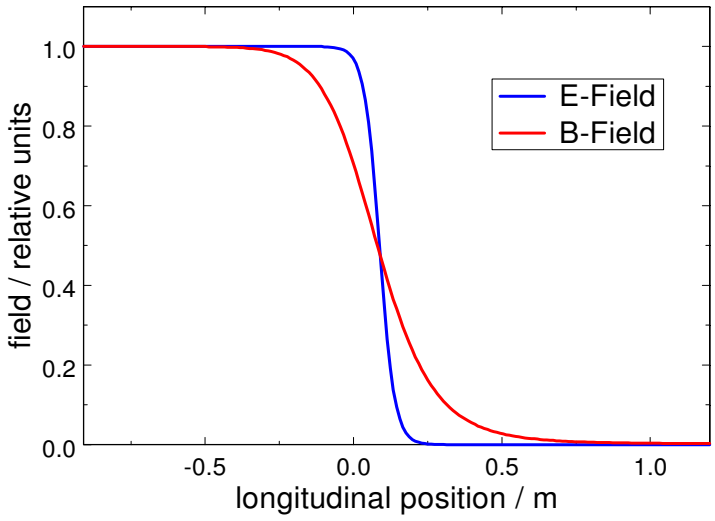

Figure 7: Electric and magnetic fields along the axis at the LISE Wien filter exit as measured and modelled with the Enge model [6]. The mismatch between the electric and magnetic fringe field causes a resolution weakening.

2.1.2 The beam physics code COSY INFINITY

The different setups of the Wien filter option have been simulated with the programme COSY INFINITY [7]. This is the first arbitrary order beam physics code. It is a DA (Differential Algebra, "automatic differentiation") based, new generation code for the study and design of beam physics systems including accelerators, spectrometers, beam lines, electron microscopes and glass optical systems. COSY has an object oriented language environment for the use of DA (as well as graphics). It is a recursive language similar to PASCAL and yet has a powerful syntax. The programme runs from many platforms and supports many graphic drivers. It is available from the site http://cosy.pa.msu.edu/ after registration. The user guide / reference manual and the programming manual can be obtained from the same location. Information about the author Martin Berz can be found on his personal homepage http://bt.pa.msu.edu/berz/. A good description of the underlying theory can be found in reference [8].
In addition to the usual six phase space coordinates the code works with a mass and a charge coordinate which are inserted into the Taylor formalism:

$$r_1 = x \qquad r_2 = a = p_x / p_0$$
$$r_3 = y \qquad r_4 = b = p_y / p_0$$
$$r_5 = l = -(t - t_0) v_0 \gamma / (1 + \gamma) \qquad r_6 = \delta_K = (K - K_0) / K_0$$
$$r_7 = \delta_m = (m - m_0) / m_0 \qquad r_8 = \delta_z = (z - z_0) / z_0$$

t : time of flight; γ : total energy over $m_0 c^2$; p : momentum; z : charge;
v : velocity; m : mass; K : kinetic energy;

Equation 1: Phase space coordinates of COSY INFINITY.

This allows the simultaneous simulation of particles having different masses. This option has been exploited in the calculations. The procedures used for the simulation are drift length (DL), electrostatic quadrupole (EQ), Wien filter (WF), electrostatic separator (ES) and magnetic dipole (DI).

2.2 General layout

A symmetric Wien filter solution has been considered where two desired masses m_1 and m_2 are split up to the left and right in respect of the forward direction. The straight-through condition is accomplished for a virtual mean mass m_m which is calculated by

$$m_m = \frac{4 m_1 m_2}{\left(\sqrt{m_1} + \sqrt{m_2}\right)^2}.$$

The schematic setup is displayed in **Figure 8**. Between the ion source and the Wien filter an electrostatic quadrupole triplet is placed. It allows the generation of a double focus behind the velocity filter which separates the two masses into two initially symmetric beam lines. To allow for an immediate insertion of elements at each beam line transverse space is attained by increasing the small separation angle of the Wien filter (usually several degrees) with electrostatic deflectors which are followed by dipole magnets. Each line has additional magnets to switch each of the beams either

to the charge breeder, which is located within the confinement area, or to the low energy experiments and mass identification, which are outside this area.

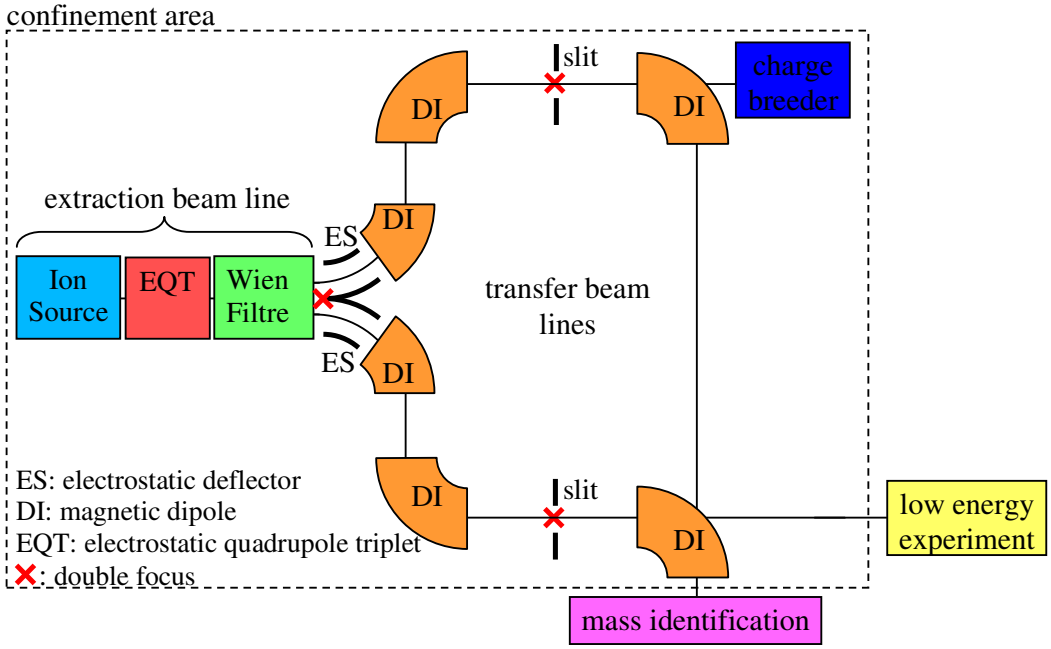

Figure 8: General layout of the Wien filter solution.

2.3 The extraction beam line

The beam optics ranging from the ion source to the end of the Wien filter for the masses A_1 = 90 and A_2 = 140 is presented in **Figure 9**. The voltages in the quadrupoles amount to several kV for an extraction voltage of 34 kV. The E-field in the 50.0 cm long Wien filter achieves 43.8 kV/m according to a voltage of 4.4 kV if the plates are installed in a distance of 10 cm. The magnetic flux is B = 0.18 T. The deflection angle behind the Wien filter is 2° leading to a separation of 5.2 cm between A_1 = 90 and A_2 = 140 in the beam focus located 50.0 cm behind the filter.

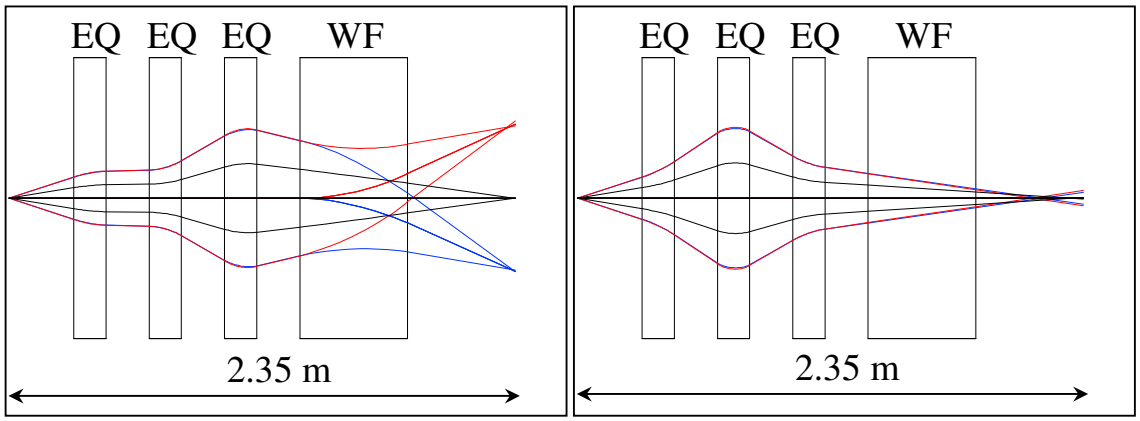

Figure 9: Transverse optics (left: horizontal, right: vertical) of section 1 ranging from the ion source to the focus behind the Wien filter.

The Wien filter itself without the subsequent dipoles has a rather weak mass resolution. In the case of the separation of A_1 = 90 and A_2 = 140 by 5 cm the mass resolution does not exceed much more than R_m = 50 assuming an entrance slit of 2 mm. The limit of the resolution is given by the fact that the velocity of particles deflected within the Wien filter is not constant but changes due to the acceleration or deceleration in the electric field. This effect is the larger the longer the filter (if fields are kept constant) and the higher the fields and avoids an arbitrary large separation of the masses. The limit evaluated also in respect of second order effects was found to be at a mass resolution of R_m = 140 corresponding to a separation of the masses A_1 = 140 and A_2 = 136 by 8 mm with a magnetic field of 0.5 T and an electric voltage of 11 kV.
The symmetric beam separation looks comfortable in respect of the beam line downstream the Wien filter as the two branches are identical reducing design effort and production costs. However, in the case of an uncontrolled breakdown of the Wien filter fields the symmetric setup bears the risk of impacting the deflector plates in the forward direction.
However, this fact does not impose a strong constraint as alternatively to the beam optics in **Figure 9** the Wien filter can be operated in an asymmetric mode, i.e. only one of the two desired masses is deviated the other one is remaining on the axis. This is shown in **Figure 10**. Here the crossed fields (B_{WF} = 394 mT, E_{WF} = 0.774 kV/cm) do not interfere with the A = 100 beam (blue rays) whereas the A = 104 beam (red rays) is deflected and has an axis offset of 10.0 mm in the focal point. In this example the focusing is achieved by several electrostatic Einzel lenses combined with a single electric quadrupole.

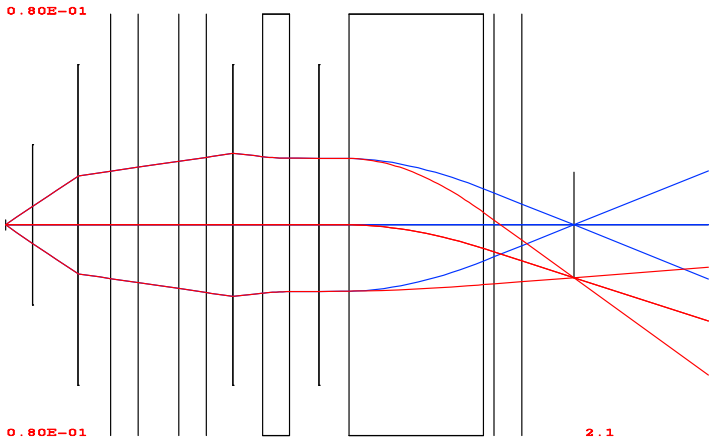

Figure 10: Asymmetric Wien filter operation. One mass (red, *A* = 104) is deviated whereas the other one (blue, *A* = 100) remains on the axis.

2.3.1 The three plug solution

To protect the surroundings against radiation and contamination the so-called plug technology developed at TRIUMF, Vancouver, has been adapted to house the target ion source assembly and the beginning of the secondary beam line. As indicated in **Figure 1** (left upper part in orange rectangular) three containment tanks referred to as "plugs" have been originally foreseen in the SPIRAL 2 design.

Each plug has an available length of 1063 mm. They have walls of 103 mm thickness and are installed in a distance of 150 mm. The first plug is to house the ion source. The others could house the beam line elements such as the electrostatic quadrupoles and the Wien filter. The design goal was hence to distribute the necessary beam line elements in a reasonable manner over the plugs.

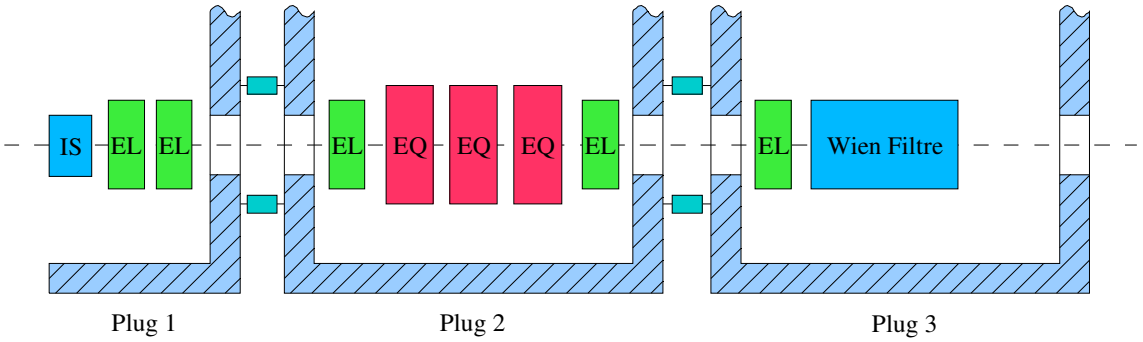

Figure 11: Setup of the three plug optics. IS: ion source, EL: electrostatic Einzel lenses, EQ: electrostatic quadrupoles.

In addition to the optical elements mentioned above the setup which takes into account the plug geometry contains several electrostatic Einzel lenses (EL in **Figure** 11). These are necessary to act against the defocusing space charge forces and to transport the beam to the next plug without losses. The space charge is mainly caused by the support gas of the source, e.g. helium *He* or oxygen O_2, which is extracted and transported with the radioactive beam up to the first magnetic element of the beam line, which is in our case the Wien filter. As all particles extracted from the source have the same electric rigidity they are not separated in the preceding electrostatic quadrupoles. An effect connected with the separation of the support gas in the Wien filter is that due to their large velocity difference the support gas ions are strongly deflected in the Wien filter and might hit the electrode. This would cause secondary electron emission, succeeded by flashovers and metal sputtering with the damage of the electrode surface as a consequence. In principle this problem can be counteracted by a special design of the electrode having an opening slit in the centre to let pass the support gas beam. The influence of such a slit on the electric field uniformity is under investigation by M. Duval [12].

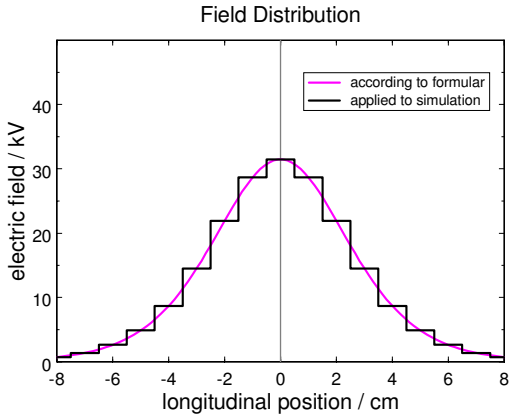

Figure 12: Longitudinal field distribution of an Einzel lens (magenta, see Appendix 9.2) approximated by a step function (black) for 100 kV supply voltage, 4 cm radius and a length of the inner tube of 1 cm.

For the simulations of the setup in **Figure 11** the programme TRANSPORT in a version from PSI Villigen has been used [9]. This version is capable to treat electrostatic elements and, if desired, takes space charge fields into account. The Einzel lenses are not available as elements but can be realised by a sequence of accelerating gaps. In this way the longitudinal field distribution for a given lens geometry, taken from analytical formulas (Appendix 9.2), can be approximated by a step function as shown in **Figure 12**.

The result of the 1st order TRANSPORT simulation including space charge is displayed in **Figure 13** for an I = 2.0 mA beam. The beam optics has waists between the plugs generated with the Einzel lenses. The asymmetric focusing of the beam in the Wien filter (weak horizontal focusing, no vertical focusing) is compensated with the quadrupole triplet in the second plug. With this a double waist can be obtained at the exit of plug 3. The separation of beam impurities occurring in the Wien filter is imitated by a stepwise reduction of the beam current according to an exponential law. Therefore the Wien filter is cut into 10 slices of 5.0 cm length each.

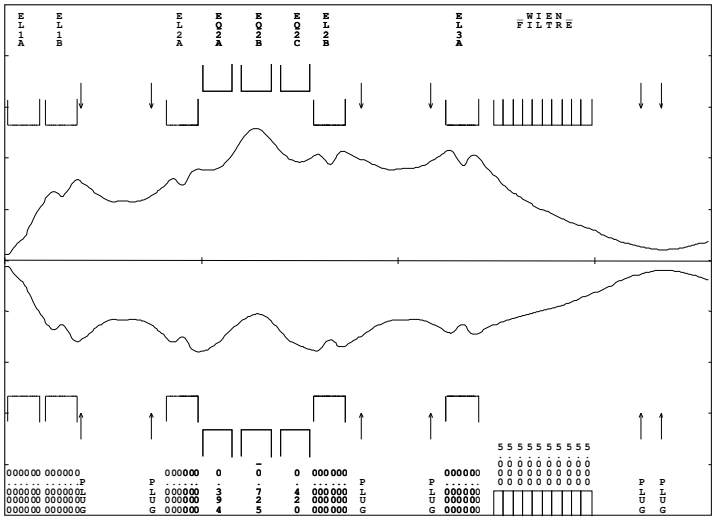

Figure 13: TRANSPORT simulation of the three plug solution. Above: vertical beam envelope. Below: horizontal beam envelope. The radius of the Einzel lenses amounts to 4.0 cm, the one of the electrostatic quadrupoles to 5.0 cm.

2.3.2 The two plug solution with focal point compensation

As the minimisation of the number of beam line elements in the confinement area is a major goal of the design a setup avoiding the third plug has been studied (**Figure** 14). In the compressed beam line the electrostatic quadrupole triplet is replaced by a single quadrupole which creates enough space to insert the Wien filter into the second plug.

The beam envelopes, calculated with TRANSPORT (**Figure 15**), now exhibit a vertical waist which is flatter and a horizontal waist which is sharper compared to the three plug solution but basically the extraction is feasible with this reduced setup.

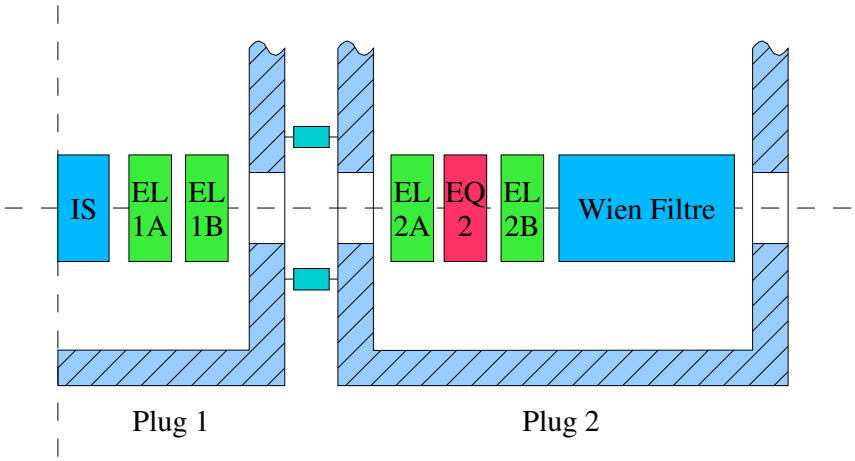

Figure 14: Two plug option with focal point compensation. The third plug has been cancelled by reducing the quadrupole triplet to a single quadrupole and shifting the Wien filter into the second plug.

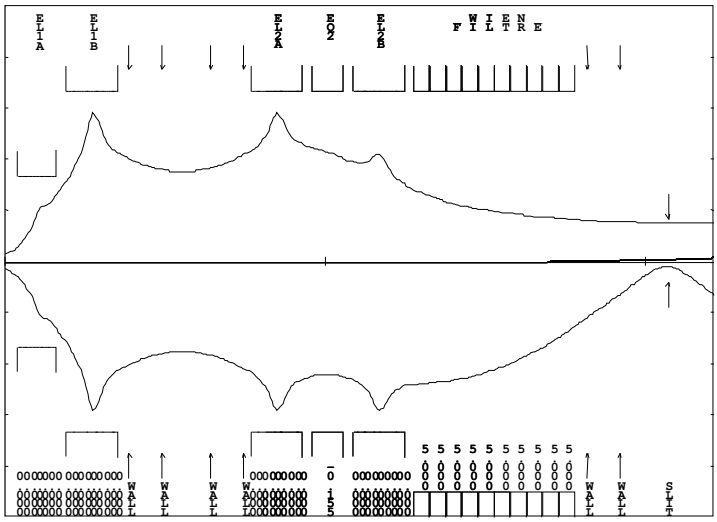

Figure 15: TRANSPORT simulation of the two plug option with focal point compensation for a beam current of I = 2.0 mA and U_{ext} = 20.0 kV. The plug walls are indicated by arrows.

2.3.3 The two plug solution without focal point compensation

The beam optics presented so far have had a combined horizontal and vertical beam waist behind the Wien filter. This property facilitates the design of the beam lines beam in the subsequent sections but is not compulsory for a successful beam transport. Abandoning this feature the remaining quadrupole in plug 2 can be removed from the beam line. A reduced arrangement, shown in **Figure 16**, which furthermore cancels one of the two Einzel lenses in the first plug, has been regarded. The removal of the Einzel lens became possible by an optimisation of the lens geometry carried out by B. Jacquot including fringe field shields. This resulted in a larger E-field on the axis and stronger focusing forces.

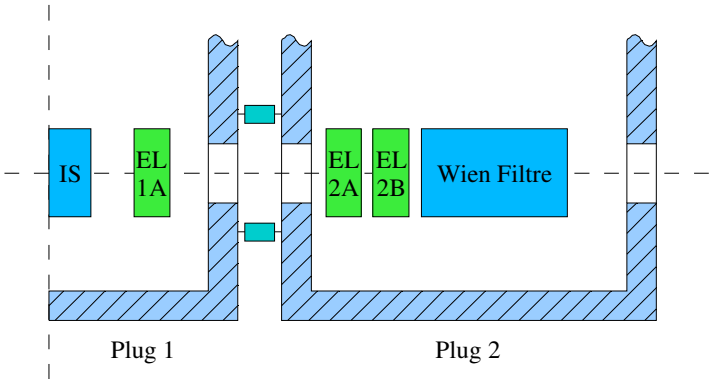

Figure 16: Two plug solution without focal point compensation. Only one Einzel lens for beam extraction is placed in the first plug, another two for beam capture and the generation of a focus behind the Wien filter in the second one.

The beam optics presented in **Figure 17** compares the behaviour of different masses in this arrangements. For lighter masses the beam foci are shifted upstream. From this calculation it is obvious that the subsequent part of the separator has to be flexible enough if it is supposed to capture masses from the whole fragment spectrum ranging from approximately A = 70 to A = 170. As described in section 2.1.1 it is possible to recover the symmetric double focus by the superposition of a quadrupole field in the Wien filter itself. As this is a space saving option it should be kept in mind for the technical design of the Wien filter.

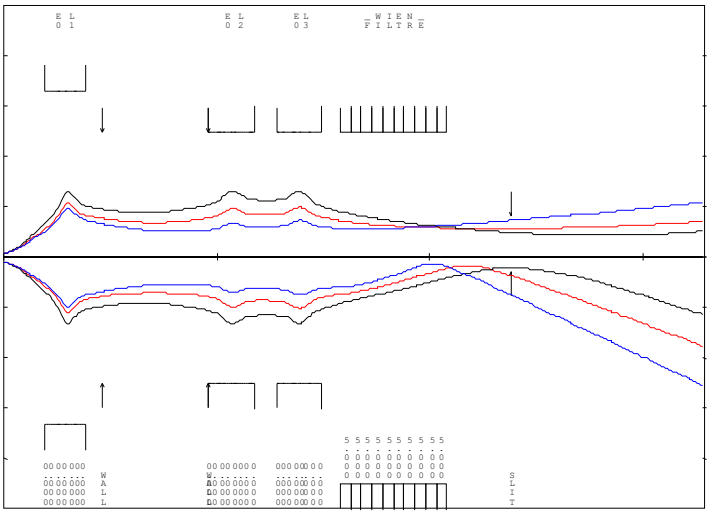

Figure 17: Horizontal (below) and vertical (above) beam envelopes in the extraction line of a beam with A = 100 (black curves), A = 40 (red curves) and A = 16 (blue curves) for an extraction voltage of U_{ext} = 60 kV and a beam intensity of I = 2.0 mA. The length of the Wien filter is L_{WF} = 500.0 mm.

2.4 The transfer beam lines

According to the Wien filter field settings the beam cocktail extracted from the 1+ source is fanned out and two radioactive beams of different masses are directed into the subsequent beam lines. One of these beam lines (beam line A) goes either to the right or straightforward and transports one beam to the charge breeder. The other beam line (beam line B) deflects the second beam to the left and redirects it to the low energy experimental hall. Except for the beam transport to the different areas of

SPIRAL 2 the transfer beam lines have to provide with the final mass resolution of at least R_m = 250 which cannot be achieved by the Wien filter alone. Three options have been elaborated which are presented in the following.

2.4.1 Option 1: Minimal setup

Option 1 of the transfer beam lines assumes a symmetric Wien filter operation. From the double or horizontal focus behind the Wien filter, depending on the precedent setup, in option 1 each beam is deflected by an 8° electrostatic deflector and after a drift by an 80° dipole magnet. The second dipole necessary to bend the beams into the direction of the charge breeder or the mass identification is a double focusing 90° magnet. The corresponding beam optics, calculated with COSY INFINITY, is shown in **Figure 18**. By simulating two beam with masses A1 = 139 and A2 = 140 simultaneously and assuming an entrance slit of 2.0 mm the mass resolution of the presented setup has been calculated. The investigation reveals that the value R_m is about 50 behind the Wien filter and 300 in the focal point behind the first dipole magnet which already satisfies the requirements. Behind the second dipole magnet the mass resolution is in the range of R_m = 600.

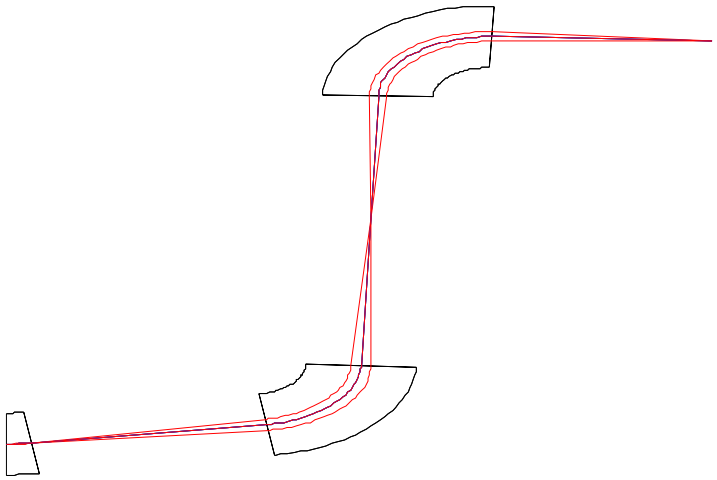

Figure 18: Horizontal optics of option 1 reaching from the electro-static deflector to the final focus.

On one hand the setup fulfils the goal of a minimal adoption of beam line elements in the confinement area. Behind the Wien filter focusing is obtained solely by double focusing dipole magnets not introducing quadrupole lenses. On the other hand changes in the focusing properties of the beam caused by space charge forces which depend on the ion mass can not be corrected. Although electrostatic deflectors are not avoided the voltages applied reach uncritical values.

2.4.2 Option 2: Beam line B without dispersion compensation

A more flexible transport line with quadrupole insertions between the dipoles has been elaborated assuming a non-symmetric Wien filter deflecting one of the desired masses to the left whereas the other one passes the filter without deviation. The forward beam line (beam line A) has been carried out elsewhere [12] and will not be further discussed here. Here only the left bent beam line (beam line B) is considered.

Some of the ideas in the arrangement proposed in [10] have been adopted for option 2 whose general layout is presented in **Figure 19**. After the beam bent to the left generated by the Wien filter further deflection by an angle of 35° is achieved by means of a cylindrical condenser. With this one attains enough space for the insertion of a magnetic quadrupole triplet which serves for the compensation of errors in the focal point of the Wien filter and generates a horizontal and vertical focus before the right bend. The scaled drawing of **Figure 20** demonstrates the geometrical feasibility of the arrangement. This first quadrupole triplet is asymmetric and has the property of a parallel-to-parallel image in the vertical plane (R_{43} = 0). This avoids too large y-beam sizes downstream. The right bend is realised by two identical 60° magnets with an entrance and exit wedge angle of 15.84° (Focal length: 727.5 mm). According to [11] this guarantees a point-to-point image in both transverse planes of the double magnet bend system. Another quadrupole triplet, which is symmetric, assures a focus at the entry of the final 90° electrostatic deflector which bends the beam to the low energy experimental hall. As input parameters of the simulation (A = 100), carried out with COSY INFINITY, the output ellipse of the TRANSPORT simulation, as listed in **Table 3**, has been taken.

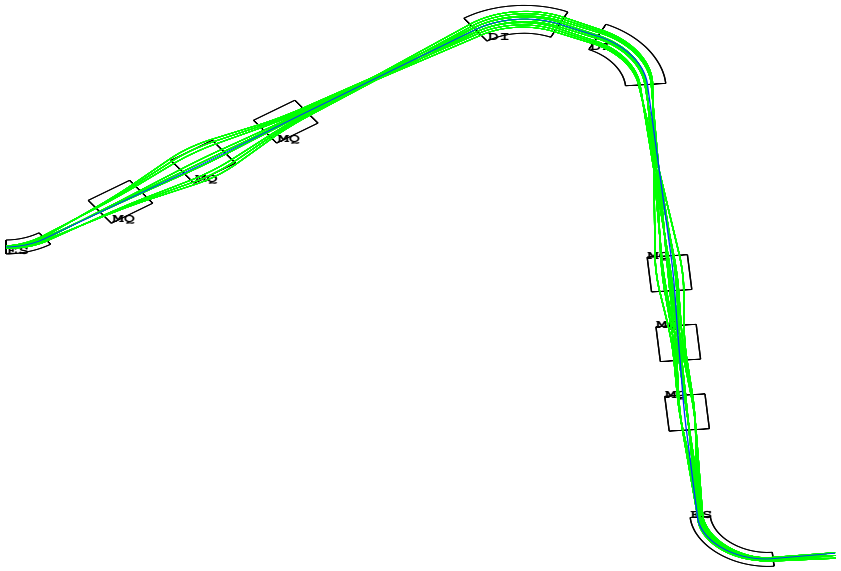

Figure 19: 2D-plot of the horizontal beam optics of beam line B.

Table 3: Input parameters of the COSY INFINITY simulation of option 2.

PARAMETER	VALUE
x_{max}	2.9 mm
x'_{max}	29.1 mrad
y_{max}	15.5 mm
y'_{max}	6.5 mrad
r_{12}	0.035
r_{34}	-0.559
r_{56}	1.000

Table 4: Properties of the beam line elements.

IDENTIFIER	PROPERTIES
ES01	Type: cylinder Bending Radius: 400.0 mm Deflection Angle: 35.0° Aperture: 20.0 mm
MQ01–MQ06	Aperture: 40.0 mm
DI01–DI02	Bending Radius: 0.5 mm Deflection Angle: 60.0° Entrance wedge angle: 15.84° Exit wedge angle: 15.84°
ES02	Type: cylinder Bending Radius: 400.0 mm Deflection Angle: 90.0° Aperture: 20.0 mm

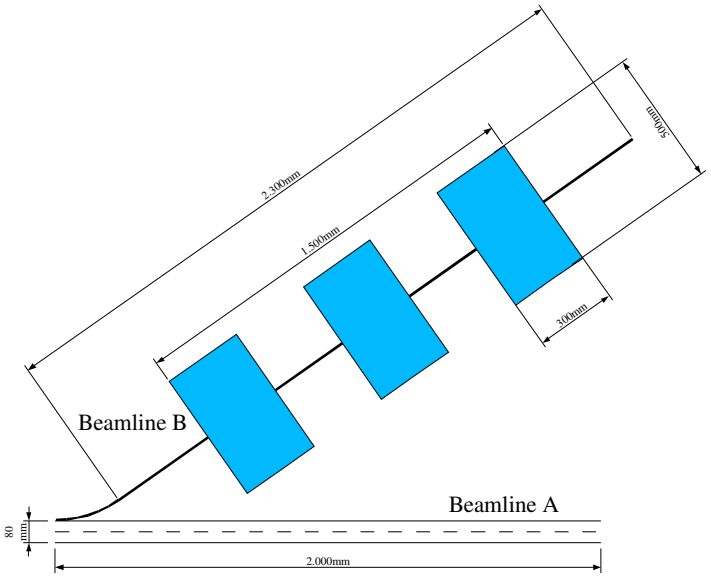

Figure 20: Geometrical verification of beam line B. The first quadrupole does not coincide with the beam tube of beam line A.

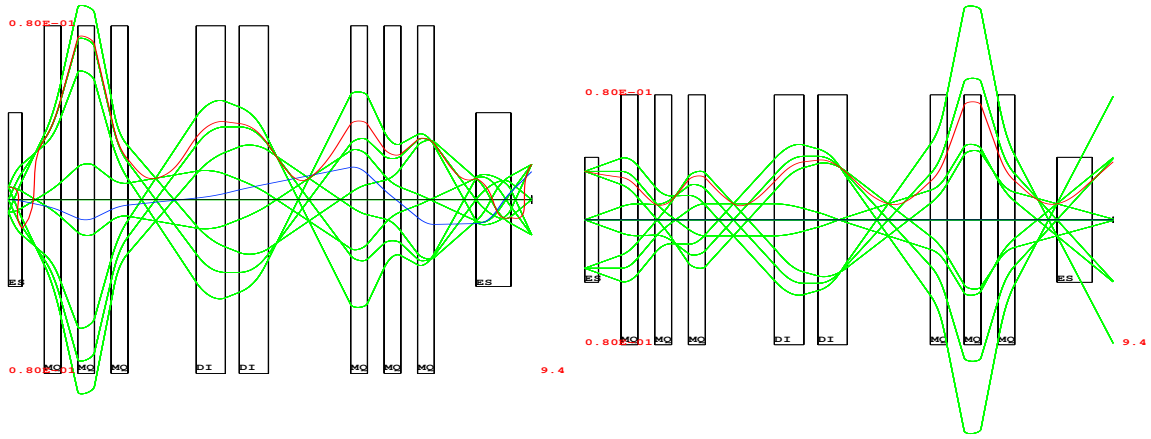

Figure 21: Horizontal beam optics of beam line B. green: rays without energy deviation; blue: ray with 1% energy deviation; red: beam envelope (ignore negative values).

2.4.3 Option 3: Beam line B with dispersion compensation

Option 3 is essentially based on Option 2 but reveals some improvements. The design proposed does not only provide a mass purification but enables the compensation of the dispersion terms (R_{16}, R_{26}, see **Table 5**) introduced by the Wien filter while keeping the beam envelope within the limits of the aperture guaranteeing a reasonable transmission.

Table 5: Momentum and angular dispersion in the focal point behind the Wien filter.

Separation	R_{16} / m	R_{26} / rad
100↔105	-0.330	-0.496
100↔110	-0.172	-0.282
100↔150	-0.044	-0.073

The beam line, illustrated in **Figure 22**, with a total length of approximately 11 m contains 16 bending and focusing elements:

- 3 electrostatic deflectors
- 7 magnetic quadrupoles
- 2 bending magnets
- 4 electrostatic quadrupoles

These elements are arranged in four sections: the electrostatic deflector, the magnetic stage, the electric stage and the beam matcher. Their design is discussed in the following subchapters.

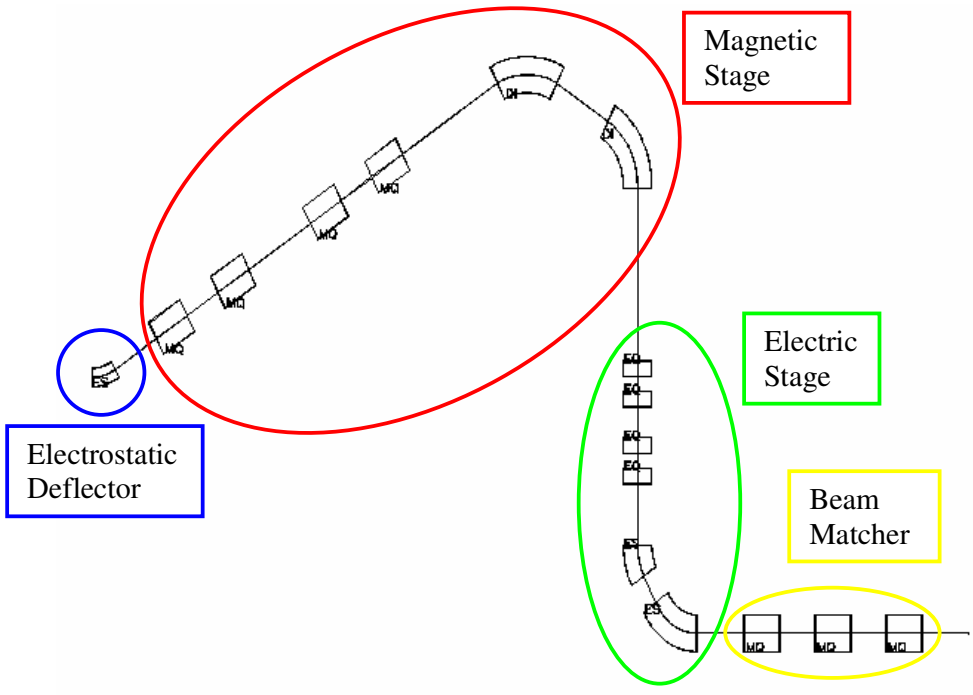

Figure 22: General Setup of beam line B. It consists of four sections: the electrostatic deflector, the magnetic stage, the electric stage and the beam matcher.

2.4.3.1 Electrostatic deflector

The beam separation obtained with the velocity filter in the focal point (30.0 cm downstream the filter) amounts just to 16 mm. With a deviation angle of approximately 2° it is from geometrical reasons not possible to insert focusing elements at the required positions without further deflecting the beam and thus gaining space between the two beam lines. Because of its compact size and well shielded fields an electrostatic deflector of spherical shape is applied for this purpose. Having a bending radius of 0.4 m it deflects the beam by 30°. Due to its spherical shape the deflector acts focusing in both transverse planes which facilitates the beam transport downstream.

2.4.3.2 Magnetic stage

The electrostatic deflector is succeeded by the magnetic separator stage. It is set up from two magnetic quadrupole doublets and two symmetrically split bending magnets. As we deal with identically charged particles (q = 1+) having experienced the same extraction voltage their momenta solely depend on their masses and hence the $B\rho = p/q$ separation in this stage is in fact a pure separation in particle mass. Regarding the optics of point like and parallel rays starting from the very beginning of the line (entrance of the electrostatic deflectors) a point-to-point image to the entrance of the first bending magnet in combination with a parallel-to-point image to a focal point placed 200.0 mm behind the second quadrupole doublet can be imposed on the beam with the four free parameters provided. The latter coincides with the focus of the following double magnetic bend system composed of two 60° dipoles each with a bending radius of ρ = 0.5 m. This system has been designed to be doubly focusing. To achieve this, entrance and exit wedge angles of 15.84° have to be chosen [11]. The focal length L_{foc} is then determined by [11]

$$L_{foc} / \rho = 1.455$$

which in our case results in L_{foc} = 727.5 mm. Initially parallel rays are imaged to a point in the focus of this double bend system whereas initially point like rays leave the magnetic stage in a convergent state.

2.4.3.3 Electric stage

The electric stage offers an additional $E\rho = pv/q$ separation to minimise the energy width of the beam and gives the possibility to compensate for the beam dispersion. It consists of two electrostatic quadrupole doublets and a double bend system made from two electrostatic deflectors of spherical shape. The settings of the quadrupoles are chosen to compensate the momentum and angular dispersion of the beam at the exit of the second deflector. Additionally a parallel image is fulfilled for initially point like rays. This constraint facilitates the beam optics design in the subsequent beam matcher section. Unlike the magnetic bend the electric bend is asymmetric and composed of a 30° and a 60° deflector with a bending radius of ρ = 0.4 m each. The asymmetric segmentation allows for a beam extraction behind the first deflector just by switching of this element. In this way the beam can be transported e.g. to the mass identification station or injected into beam line A.

2.4.3.4 Beam matcher

The beam matcher is the final stage of the beam line. It comprises a magnetic quadrupole triplet. It generates a final focus combined with a point-to-point image. Although underdetermined (four constraints versus three free parameters) this goal can be achieved within good accuracy. From here the beam can either be trapped, further guided to the experimental hall or bombarded directly onto a target.

2.4.3.5 Beam optics summary

The results of the beam optics calculated with the code COSY INFINITY is presented in the following figures. **Figure 23** displays the horizontal and **Figure 24** the vertical beam optics of initially point like and parallel rays. In addition the beam envelope (in red) is plotted. In **Figure 25** the dispersion (in blue) is shown. As the course of the dispersion strongly depends of the initial conditions several points of analysis at which a large dispersion and a small beam size coincide have to be provided. For instance, in the case of separating mass 100 and 150 a position in the drift between the magnetic and electric stage could be chosen (presumably the focus of the double magnet system). For the other two separations an analysis point in between the two dipole magnets would be more appropriate.

Mass separation: 100↔150

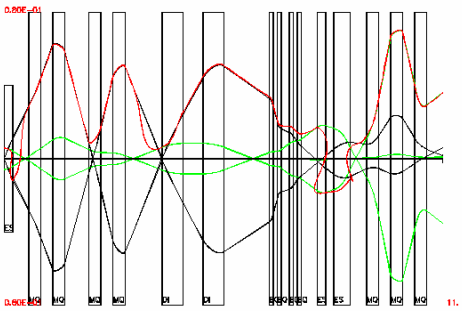

Mass separation: 100↔110

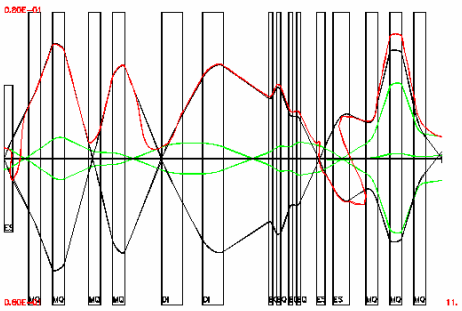

Mass separation 100↔105

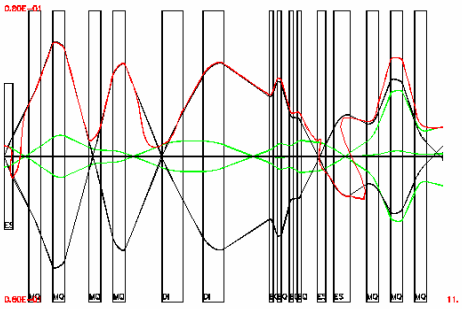

Figure 23: Horizontal beam optics of beam line B. Black: initially point like rays. Green: initially parallel rays. Red: beam envelope (ignore negative values).

Mass separation: 100↔150

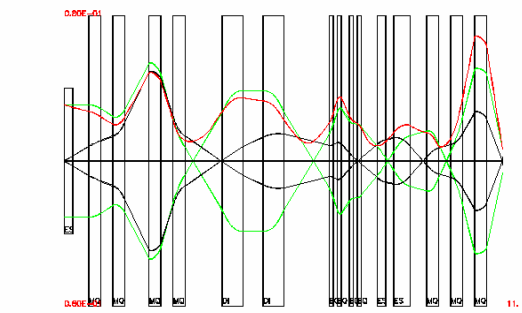

Mass separation: 100↔110

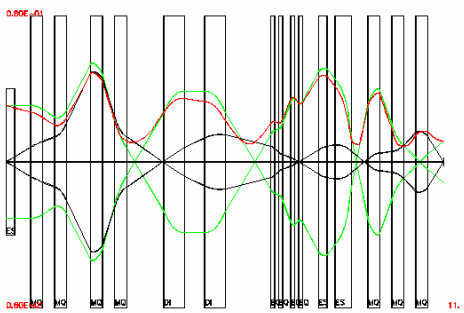

Mass separation 100↔105

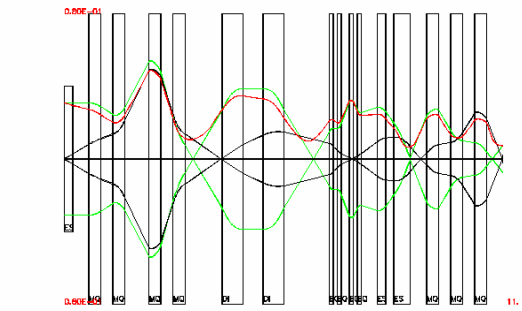

Figure 24: Vertical beam optics of beam line B. Black: initially point like rays. Green: initially parallel rays. Red: beam envelope.

Mass separation: 100↔150

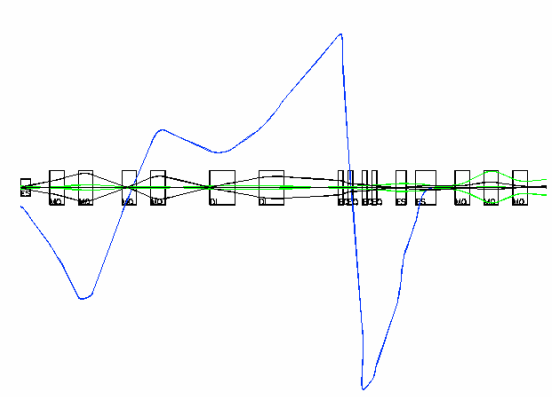

Mass separation: 100↔110

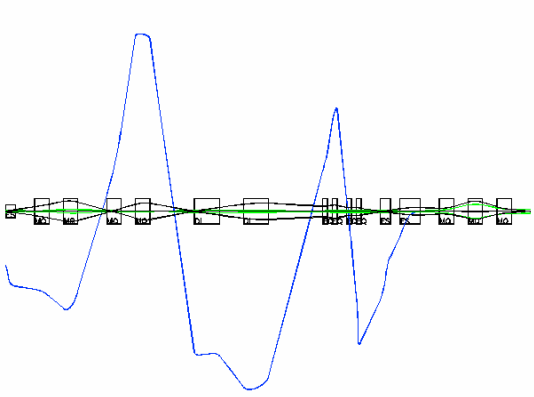

Mass separation 100↔105

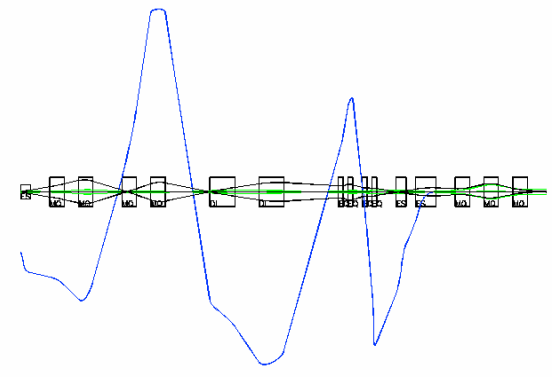

Figure 25: Dispersion (trajectory of particle with $\Delta p/p = 1$) in beam line B. With the presented setup the initial beam dispersion which depends on the mass separation of the Wien filter can be compensated.

Part 2: A multi charge ion recirculator for the charge breeder

3 Introduction

Ions of high charge states as required for both stable and radioactive beams in order to optimally profit from the accelerating voltage provided can be produced by means of charge state breeders. However, the energy increase obtained is accompanied by an intensity decrease due to the low efficiency of the charge breeding process itself. With respect to the production of radioactive beams an enhancement of the breeding efficiency would be most desirable to avoid a high power primary beam as yet inevitable to counteract the loss in intensity. For this purpose the beam optics of an ion recirculation capable to separate the desired charge state and to reinject the remaining charge spectrum has been designed. The ions, potentially extracted from both sides of the charge breeder, are focused by means of electrostatic quadrupole doublets and bent by two 180° dipole magnets resulting in a racetrack-like shape. After one revolution the optics realises horizontally and vertically a point-to-point image independent from the charge state of the ions. The second order geometric aberrations as well as most of the chromatic aberrations vanish. The non-zero energy dependant aberrations are compensated by the charge dependant aberrations leading to an effectively achromatic system up to the second order. The beam optical calculations have been carried out with the arbitrary order beam physics code COSY INFINITY and been validated with the beam envelope code TRANSPORT.

The efficiency of charge breeders is essentially limited by two effects. On the one hand the ions are generated in a broad spectrum of different charge states where most of them are lost in a post-source spectrometer. On the other hand, caused by the symmetric potential distribution of ECR ion sources, often applied for charge breeding, the ions are not only extracted in the forward but ineluctably also in the backward direction. As a consequence the efficiency yields obtained by high performance sources do not exceed 2-7% for metal ions and approximately 10% for gaseous elements [13]. Following an idea by E.A. Lamzin [14] the possibility of reinjecting the undesirable ions from both sides of the booster would solve both deficiencies and would lead to a tremendous increase of the charge breeding efficiency. In RIB-facilities, high power primary beams with their challenges in respect of operational safety and radiation protection could thus be avoided. It should be mentioned that such an ion recirculation has never been technically realised.

The poster of the EPAC conference 2004 dealing with this subject is added to this report as Appendix 0.

4 General Layout

In contrast to reference [14] where the ion recirculation is obtained by means of an electrostatic ring and the expansion of the charge states by a separated magnetic spectrometer the setup proposed here combines ion recirculation and charge state separation by applying two 180° dipole magnets with field index $n=0$. Electrostatic

elements are solely used for beam focusing. For this purpose four quadrupoles (EQ01, EQ02, EQ03, EQ04), arranged in doublets, are placed between the ion source and each of the dipoles. Due to the charge dispersion the back straight is exempt from focusing elements.

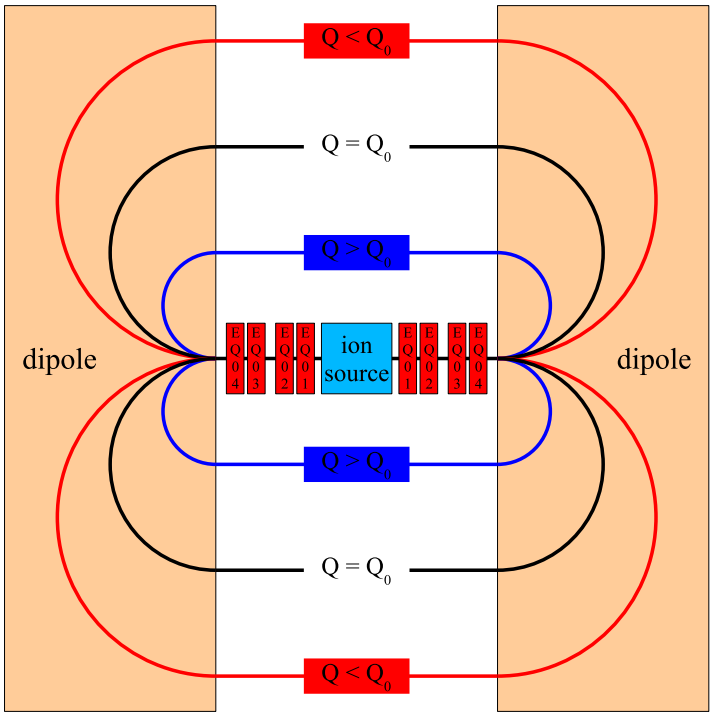

Figure 26: Racetrack shaped ion recirculator. *Q*: arbitrary charge; Q_0: reference charge; EQ: electric quadrupoles.

To achieve the design goal of recirculating a spectrum of $^{140}_{54}Xe^{q}$ ranging from q = 1+ to q = 40+ with a bending radius of the reference charge state q_0 = 20+ of R_{q0} = 0.5 m and a spacing between the closest charge states (q = 39+, 40+) of at least Δx = 1.0 cm the width of the two magnets reaches 10.0 m and the depth 3.0 m (each with margin included). The distance between the two dipoles defined by the minimum space necessary for the insertion of the ion source and the electrostatic quadrupoles amounts approximately to 4.0~m. With this, the whole arrangement has a quadratic shape of 10×10 m². However, these dimensions could be diminished by choosing less ambitious design parameters.
Regarding the slowest particle (q = 1+) and assuming an extraction voltage of U_{ext} = 20 kV we find a time-of-flight between charge breeder extraction and reinjection of $\tau \cong 130$ µs which is much less than the fastest confinement times obtained for state-of-the-art ECR sources lying in the range of several tens of milliseconds [15] and moreover far below the half-life of $^{140}_{54}Xe$, $T_{1/2}$ = 13.6 s.

5 Theoretical Considerations

A recycling system allowing to extract the desired charge state q_0 and to recirculate all other charge states q into the charge breeder can be modelled by a flow chart as displayed in **Figure 27**. The initial 1+ beam current i_{in} is injected into the charge breeder where the desired charge state is bred with the breeding rate β. The desired q_0 beam can be extracted from the system with a certain extraction efficiency ε

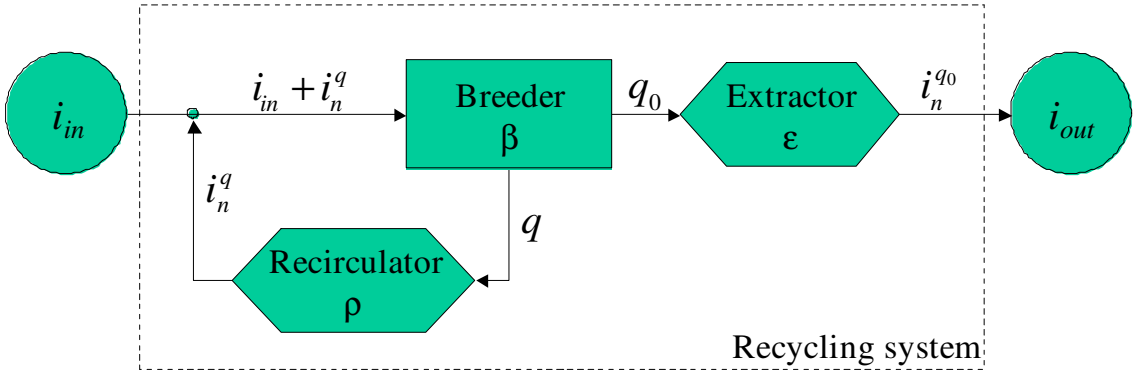

Figure 27: Flow chart of a ion recycling system with charge breeder, extractor and recirculator.

resulting in the current $i_0^{q_0} = \beta \cdot \varepsilon \cdot i_{in}$ after the first pass. Charge states $q \neq q_0$ can be reinjected with a recirculating efficiency ρ. The resulting beam current $i_1^q = (1-\beta) \cdot \rho \cdot i_{in}$ is added to the 1+ beam of the next cycle, i.e. i_{in} has to be replaced by $i_{in} + i_1^q$. After an arbitrary number of revolutions n the two coupled recursive formula describing the system are:

$$\boxed{\begin{aligned} i_{n+1}^{q_0} &= \beta \cdot \varepsilon \cdot (i_{in} + i_{n+1}^q) \\ i_{n+1}^q &= (1-\beta) \cdot \rho \cdot (i_{in} + i_n^q) \,. \end{aligned}}$$

The global efficiency of such a recycling system after n cycles can be defined as

$$\eta_n = \frac{i_n^{q_0}}{i_{in}} \,.$$

In the limit $n \to \infty$ an equilibrium is reached and one can set $i_{n+1}^q = i_n^q$ and $i_n^{q_0} = i_{out}$. With this one obtains for the equilibrated efficiency

$$\boxed{\eta_\infty = \frac{\beta \cdot \varepsilon}{1 - \rho \cdot (1-\beta)}} \,.$$

The temporal behaviour of η_n and the dependence of the equilibrated efficiency η_∞ are plotted in **Figure 28** for different values of the breeding rate and the extraction and recirculation efficiency. Part (a) refers to ideal values of ε = 1 and ρ = 1, part (b) to more realistic values of ε = 0.8 *and* ρ = 0.8. Depending on the parameters the equilibrium state is reached after 200 cycles or earlier which is in the order of two seconds if one assumes a breeding and recycling time in the order of 10 ms. The final efficiency initially increases slightly with the recirculating efficiency up to ρ = 0.8 but increases dramatically for values 0.8 < ρ < 1.0. High over all efficiencies can hence only be obtained if substantial losses during the recirculating process as well as in the extraction line can be avoided.

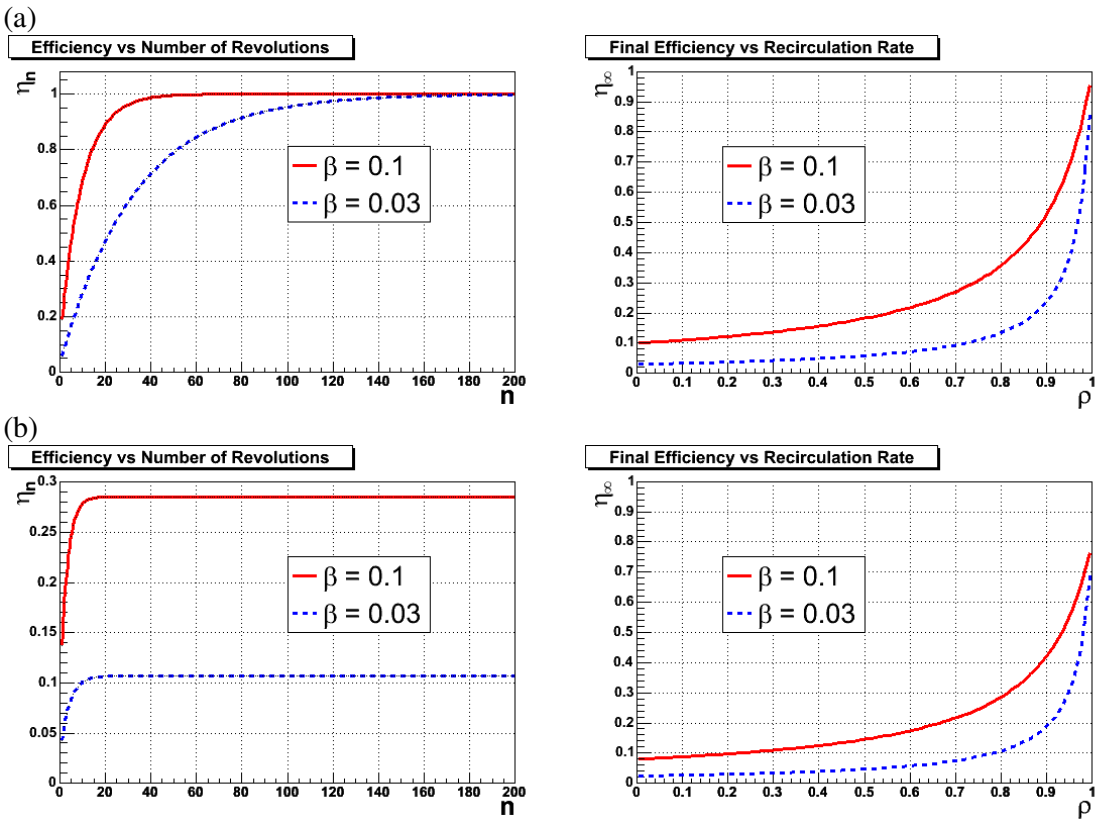

Figure 28: Efficiencies of ion recirculation versus number of cycles (left) and recirculation rate (right) for (a) ideal values of recirculation and extraction rates $\varepsilon = 1$ and $\rho = 1$ and (b) realistic values $\varepsilon = 0.8$ and $\rho = 0.8$.

6 Beam Optical Calculations

The beam optics envisaged with the described setup is a combined point-to-point, parallel-to-parallel image, resulting in a waist-to-waist image, in both transversal planes from the source extraction to the reinjection. Except for the vertical parallel-to-parallel image this optics is independent from the ion charge. The settings of the electrostatic quadrupoles are symmetric with respect to the charge breeder but uncoupled at each side. They deliver four free parameters for the minimisation of the transfer matrix elements R_{12}, R_{34}, R_{21} and R_{43} in first order calculations and the transverse beam envelopes Σ_{21} and Σ_{43} or the end positions and angles of rays for higher orders. Two different set of parameters, referred to as optics 1 and optics 2, which fulfil the conditions with sufficient accuracy have been elaborated. Both Optics exhibit a transversal waist in the beam line between charge breeder and dipole magnet: optics 1 in the vertical plane, optics 2 in the horizontal plane.

Horizontal waists within the bending section and a double waist at half optical path length on the back straight are common to both optics and could serve as recirculator injection and extraction points by means of electrostatic septa. The input parameters for the calculations can be taken from table **Table 6**. As we deal with an electrostatic acceleration the particles have all the same electric rigidity $E\rho = 2 \cdot U_{ext}$

but due to $B\rho = p/Q$ different magnetic rigidities. The initial beam parameters are typical values obtained for ECR charge breeders [15].

Table 6: Input parameter for the beam optical calculations.

PARAMETER	VALUE
Particle	
mass number	A = 140 (e.g. $^{140}_{54}Xe$)
charge	Q = +20, +1, +40 e
kinetic energy	E_{kin} = 400.0, 20.0, 800.0 kV
electric rigidity	$E\rho$ = 40.0 kV
magnetic rigidity	$B\rho$ = 0.054, 0.241, 0.038 Tm
Beam	
radius	R = 4.0 mm
opening angle	$\alpha = \pm 10$ mrad
emittance	ε = 40.0 πmm·mrad

6.1 COSY INFINITY Simulations

COSY INFINITY [7] (in the following referred to as "COSY") is an arbitrary order beam physics code. It is based on differential algebra and adapted for the study and design of beam physics systems including accelerators, spectrometers and beam lines. It offers the option to simultaneously simulate particles with different masses or charges states, the latter being of especial interest for the problem at hand.

The calculations presented here have been carried out in 3rd order. The quadrupoles settings could be optimised by means of the built in algorithms. In **Figure 29** (a) the horizontal beam optics 1 of the charge states q = 16+ (red), q = 20+ (black) and q = 24+ (blue) is shown in a 2D-rays-illustration. Apparently this optics is independent from the charge state, as the longer trajectory in the dipole magnet is compensated by the likewise increased weak focusing. The vertical optics 1 (parallel and point rays) of the reference charge Q_0 = 20 e is presented in **Figure 29** (b). For charges $Q \neq Q_0$, not included in **Figure 29** (b), no compensation of variations in the trajectory length takes place in this plane due to the absence of the vertical focusing forces at the dipole edges (wedge angle $\varphi = 0°$) and the vertical waist on the back straight is consequently shifted downstream for charges $Q > Q_0$ respectively upstream for $Q < Q_0$. In the latter case this entails a strong blow up of the beam towards the end of the circulation but the envelope remains within a radius of 6.0 cm. To prevent beam losses the aperture R of the electrostatic quadrupoles has therefore been chosen to R = 10 cm.

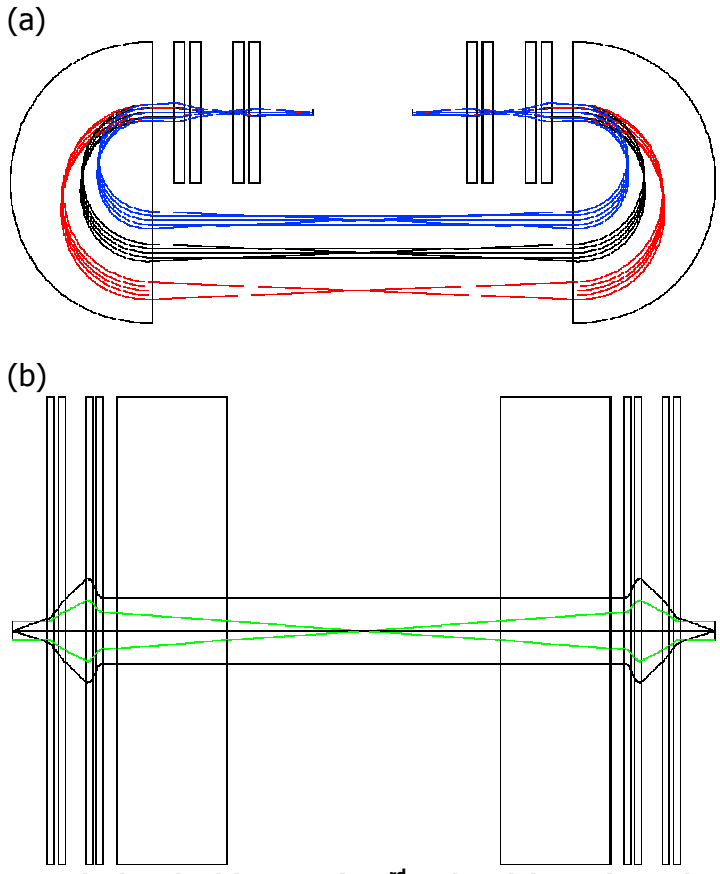

Figure 29: Optics 1 calculated with COSY in 3rd order. (a): Horizontal 2D-illustration for $Q = 16\ e$ (red), $Q = 20\ e$ (black) and $Q = 24\ e$ (blue). (b): Vertical rays of the reference charge $Q_0 = 20\ e$ (black, green).

6.2 TRANSPORT simulations

So far the influence of space charge effects has been omitted in our calculations even though the beam current may reach values of several 100 µA [15]. The main contribution of the current originates from impurities consisting of the support gas of the ion source such as ^{4}He or ^{16}O. Although having different masses than the desired beam these ions posses the same electrostatic rigidity. They are hence transported up to the dipole magnet where they are finally separated from the beam due to their different magnetic rigidity. To simulate this effect which is not a priori negligible the code TRANSPORT [16] has been consulted. The PSI version "Graphic TRANSPORT" [9] does not only offer a user friendly graphical user interface but in particular a first order space charge calculation realised by a series of thin lenses placed at user defined intervals.

The beam optics has been calculated only for half of a revolution, i.e. two quadrupole doublets, one dipole magnet and half of the back straight, corresponding to the symmetry element of the ion recirculator. This implies a point-to-parallel and a parallel-to-point image which again implies a waist-to-waist image. Both optics already observed with COSY have been confirmed by the TRANSPORT optimiser. The result of this simulation for beam optics 2 is presented in **Figure 30**. The calculation

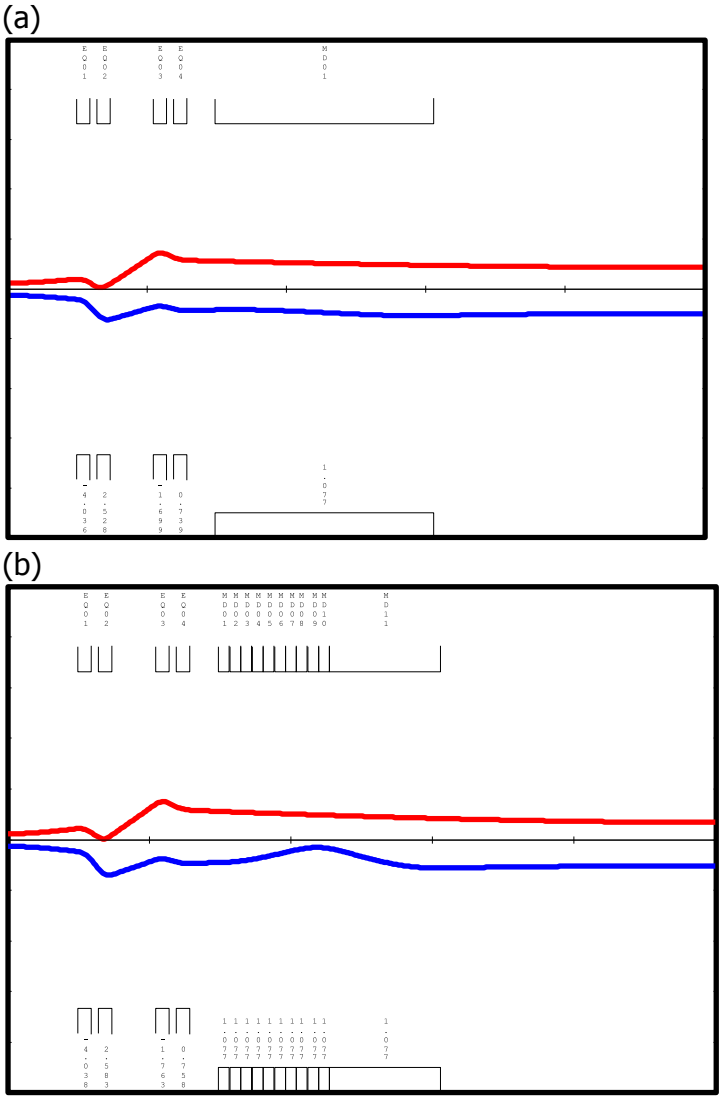

Figure 30: Beam envelopes of optics 2 for one symmetry element calculated with Graphic TRANSPORT in 2nd order without space charge (a) and in 1st order for a beam intensity of I = 1.0 mA (b).

without space charge effects, cf. **Figure 30** (a), has been carried out in 2nd order which is the maximum order implemented in the PSI version. Using the space charge option the calculation is limited to the 1st order. The result for a beam intensity of I = 1.0 mA is shown in **Figure 30** (b). The decay of the beam intensity in the dipole magnet due to the beam separation has been approximately imitated by cutting the magnet into segments and decreasing the beam intensity behind each segment according to an exponential law. The simulation proves that a modification of the beam line arrangement due to space charge effects is dispensable as the desired optics can be restored by simply readjusting the quadrupole voltages.

7 Comparison and Conclusion

The beam optics of an ion recirculator for charge breeders consisting of two 180° dipole magnets and eight electrostatic quadrupoles has been investigated with the

codes COSY and TRANSPORT. The comparison of the results is resumed in **Table 7**. An agreement in the per cent range is observed between COSY and TRANSPORT (I = 0 mA). The voltages necessary to focus a space charge beam with I = 1.0 mA rest within reasonable limits according to the TRANSPORT simulation. The concept is promising and the work should be continued to arrive at a technical realisation.

Table 7: Comparison of the quadrupole pole tip voltages obtained with COSY (reference) and TRANSPORT (with and without space charge).

QUADRUPOLE		**EQ1**	**EQ2**	**EQ3**	**EQ4**
Optics 1					
COSY ☑3rd order	kV	+10.9	-2.3	-8.4	+8.4
TRANSPORT ☑2nd order	%	-0.3	-7.6	+2.4	+0.2
TRANSPORT ☑1st order ☑space charge	%	+4.3	+4.3	+5.5	+5.2
Optics 2					
COSY ☑3rd order	kV	-20.1	+12.5	-8.4	+3.6
TRANSPORT ☑2nd order	%	+0.4	+1.5	+0.7	+2.0
TRANSPORT ☑1st order ☑space charge	%	+0.5	+3.7	+4.5	+4.6

8 References

[1] *The SPIRAL 2 Project Intermediate Report*, CEA, CNRS, IN2P3, December 2003.

[2] J. Borggreen, B. Elbek and L. Perch Nielsen, *A Proposed Spectrograph for Heavy Particles*, Nuclear Instruments and Methods, Vol. 24 (1963), pp. 1–12.

[3] J.M. Nitschke, *BRAMA, A Broad Range Atomic Mass Analyser for ISL*, Particle Accelerators, Vol. 47 (1994), pp. 153–158.

[4] *Handbook of charged particle optics*, CRC press, ed. J. Orloff, 1997, pp. 63–65.

[5] J.D. Jackson, *Classical Electrodynamics*, John Wiley & Sons, Inc., 1974, pp. 582–584.

[6] H.A. Enge, *Deflecting magnets, in Focusing of Charged Particles*, ed. A. Septier, Vol. II, pp. 203–264, Academic Press Inc., 1976.

[7] *COSY INFINITY Version 8.1 User's Guide and Reference Manual*, M. Berz, MSUHEP-20704, Department of Physics and Astronomy, Michigan State University, 2002.

[8] *Modern Tools for Particle Tracking, F. Willeke,* CERN Accelerator School, 5th Advanced Accelerator Physics Course, 1995.

[9] PSI Graphic Transport Framework by U. Rohrer based on a CERN-SLAC-FERMILAB version by K.L. Brown et al., December 2003.

[10] H. Sunaoshi et al., Nucl. Instr. and Meth. in Phys. Res. B70 (1992) 421–426.

[11] M. Fujioka et al., Nucl. Instr. and Meth. in Phys. Res. A309 (1991) 600–602.

[12] B. Jacquot, R. Cee, M. Duval, *Beam lines for radioactive nuclei*, Design notes for the Wien filter option.
[13] T. Lamy et al., *Charge Breeding Method Results with the PHOENIX Booster ECR Ion Source*, 8th European Particle Accelerator Conference, Paris, France, 3–7 June (2002) 1724–1726.
[14] E.A. Lamzin et al., *Some Methods of Generation of Multicharged Ions of Radioactive and Stable Isotopes*, 6th European Particle Accelerator Conference, Stockholm, Sweden, 22–26 June (1998), 1406–1408.
[15] *Charge Breeding*, European Commission-RTD Project, Contract HPRI-CT-1999-50003, Final Report, 1 March 2004.
[16] K.L. Brown, D.C. Carey, F.Ch. Iselin, R. Rothacker, *TRANSPORT: a computer program for designing charged particle beam-transport systems; rev. version,* CERN Report 80-04, 1980.
[17] *Elektronik des Einzelektrons,* F. Ollendorff, (1955) Springer, Wien.
[18] *Aberration Theory in Electron Optics*, X. Jiye, Advances in Electronics and Electron Physics, Supplement 17. Academic Press, Orlando, Florida, 1986.

9 Appendix

9.1 Definitions of the mass resolution

In literature many types of mass resolution are used. Their definitions are listed here:

1. Mass resolving power: $\left|\frac{D_m}{M_x}\right|$, where D_m denotes the mass dispersion and M_x the horizontal magnification.
2. Mass resolution: $R_m = \left|\frac{D_m}{M_x \Delta x_{slit}}\right|$, where Δx_{slit} denotes the entrance slit width.
3. FWHM of the mass distribution: $\delta_m = \frac{1}{R_m} = \left|\frac{M_x \Delta x_{slit}}{D_m}\right|$

As example the relation for Δx_{slit} = 2 mm is given:

if $\left|\frac{D_m}{M_x}\right|$ =1 mm / per mil $\Rightarrow$ R_m = 500 $\Rightarrow$ $\delta_m = \frac{1}{500}$

9.2 Models for the longitudinal potential distribution in Einzel lenses

A) Model by F. Ollendorf Ref.[13]:
The potential on the axis of a tube lens (two tubes) behaves like:

$$V_a(s) = \frac{V_1 + V_2}{2} + \frac{V_1 - V_2}{2} \tanh\left(2.64 \frac{s}{D}\right),$$

where V_1 and V_2 are the supply potentials of the two tubes, D is the tube diameter (identic for both tubes) and s denotes the longitudinal position on the axis with the origin in the centre of the gap.

1. Model by X. Jiye Ref.[18]:

$$V(s) = -\frac{V_0}{2\omega c / d}\left\{\ln\left(\frac{\cosh(\omega(s+L/2)/d)}{\cosh(\omega(s+L/2+c)/d)}\right)+\ln\left(\frac{\cosh(\omega(s-L/2)/d)}{\cosh(\omega(s-L/2-c)/d)}\right)\right\}$$

V_0 : potential of inner tube (outer tubes on ground) d : tube radius

ω : constant; $\omega = 1.315$ L : length of inner tube

c : gap length

9.3 Setup of the three plug solution

Result			
Element	**Length in mm**	**Radius in mm**	**Voltage in kV**
Plug 1			
drift space	17.5		
Einzel lens	160.0	40.0	100.0
drift space	35.0		
Einzel lens	160.0	40.0	125.0
drift space	17.5		
drift space	178.0		

Result			
Element	**Length in mm**	**Radius in mm**	**Voltage in kV**
Plug 2			
drift space	178.0		
drift space	80.0		
Einzel lens	160.0	40.0	80.0
drift space	19.0		
el.stat. quadrupole	150.0	50.0	0.394
drift space	50.0		
el.stat. quadrupole	150.0	50.0	-0.725
drift space	50.0		
el.stat. quadrupole	150.0	50.0	0.420
drift space	19.0		
Einzel lens	160.0	40.0	71.5
drift space	80.0		
drift space	178.0		

Result			
Element	**Length in mm**	**Radius in mm**	**Voltage in kV**
Plug 3			
drift space	178.0		
drfit space	80.0		
Einzel lens	160.0	40.0	95.0
drift space	80.0		
Wien filtre	500.0	40.0	0.5 Tesla
drift space	248.0		
drift space	103.0		

9.4 Setup of the two plug solution

Setup		
Element	**Length in mm**	**Radius in mm**
Pug 1		
drift space	40.0	
einzel lens	120.0	20.0
drift space	30.0	
einzel lens	160.0	40.0
drift space	40.0	
drift space	178.0	

Setup		
Element	**Length in mm**	**Radius in mm**
Pug 2		
drift space	178.0	
drift space	19.0	
einzel lens	160.0	40.0
drift space	30.0	
el.stat. quadrupole	100.0	40.0
drift space	30.0	
einzel lens	160.0	40.0
drift space	30.0	
Wien filtre	500.0	40.0
drift space	39.0	
drift space	178.0	
drift space	225.0	

9.5 List of beam line elements for beam line B (option 2)

Beamline Element	Identifier	Start Position	Length	End Position
		mm	mm	mm
Electrostatic Deflector	ES01	0	244,4	244,4
Drift	DL01	244,4	400	644,4
Magnetic Quadrupole	MQ01	644,4	300	944,4
Drift	DL02	944,4	300	1244,4
Magnetic Quadrupole	MQ02	1244,4	300	1544,4
Drift	DL03	1544,4	300	1844,4
Magnetic Quadrupole	MQ03	1844,4	300	2144,4
Drift	DL04	2144,4	400	2544,4
Drift	DL05	2544,4	727,5	3271,9
Magnetic Dipole	DI01	3271,9	523,6	3795,5
Drift	DL06	3795,5	250	4045,5
Magnetic Dipole	DI02	4045,5	523,6	4569,1
Drift	DL07	4569,1	727,5	5296,6
Drift	DL08	5296,6	500	5796,6
Magnetic Quadrupole	MQ04	5796,6	300	6096,6
Drift	DL09	6096,6	300	6396,6
Magnetic Quadrupole	MQ05	6396,6	300	6696,6
Drift	DL10	6696,6	300	6996,6
Magnetic Quadrupole	MQ06	6996,6	300	7296,6
Electrostatic Deflector	ES02	7296,6	628,3	7924,9
Drift	DL11	7924,9	371,6	8296,5

9.6 List of beam line elements for beam line B (option 3)

Beamline Element	Identifier	Angle	Radius	Length	Start Position	End Position
		°	mm	mm	mm	mm
Electrostatic Deflector	ES01	30,00	400,00	209,44	0,00	209,44
Drift	DL01			400,00	209,44	609,44
Magnetic Quadrupole	MQ01			300,00	609,44	909,44
Drift	DL02			300,00	909,44	1209,44
Magnetic Quadrupole	MQ02			300,00	1209,44	1509,44
Drift	DL03			600,00	1509,44	2109,44
Magnetic Quadrupole	MQ03			300,00	2109,44	2409,44
Drift	DL04			300,00	2409,44	2709,44
Magnetic Quadrupole	MQ04			300,00	2709,44	3009,44
Drift	DL04			925,00	3009,44	3934,44
Magnetic Dipole	DI01	60,00	500,00	523,60	3934,44	4458,04
Drift	DL06			500,00	4458,04	4958,04
Magnetic Dipole	DI02	60,00	500,00	523,60	4958,04	5481,64
Drift	DL07			1125,00	5481,64	6606,64
Electric Quadrupole	EQ01			100,00	6606,64	6706,64
Drift	DL08			100,00	6706,64	6806,64
Electric Quadrupole	EQ02			100,00	6806,64	6906,64
Drift	DL09			200,00	6906,64	7106,64
Electric Quadrupole	EQ03			100,00	7106,64	7206,64
Drift	DL10			100,00	7206,64	7306,64
Electric Quadrupole	EQ04			100,00	7306,64	7406,64
Drift	DL11			400,00	7406,64	7806,64
Electrostatic Deflector	ES02	30,00	400,00	209,44	7806,64	8016,08
Drift	DL12			200,00	8016,08	8216,08
Electrostatic Deflector	ES03	60,00	400,00	418,88	8216,08	8634,96
Drift	DL13			400,00	8634,96	9034,96
Magnetic Quadrupole	MQ05			300,00	9034,96	9334,96
Drift	DL14			300,00	9334,96	9634,96
Magnetic Quadrupole	MQ06			300,00	9634,96	9934,96
Drift	DL15			300,00	9934,96	10234,96
Magnetic Quadrupole	MQ07			300,00	10234,96	10534,96
Drift	DL16			400,00	10534,96	10934,96

9.7 Poster of the EPAC conference 2004, Lucerne, Switzerland

Beam Optical Design of a Multi Charge Ion Recirculator for Charge Breeders

R. Cee, W. Mittig, A.C.C. Villari*

Grand Accélérateur National d'Ions Lourds, BP 55027, 14076 CAEN Cedex 5, France

*e-mail: cee@ganil.fr

Abstract

Ions of high charge states as required for both stable and radioactive beams in order to optimally profit from the accelerating voltage provided can be produced by means of charge state breeders. However, the energy increase obtained is accompanied by an intensity decrease due to the low efficiency of the charge breeding process itself. With respect to the production of radioactive beams an enhancement of the breeding efficiency would be most desirable to avoid a high power primary beam as yet inevitable to counteract the loss in intensity. For this purpose the beam optics of an ion recirculation capable to separate the desired charge state and to reinject the remaining charge spectrum has been designed. The ions, potentially extracted from both sides of the charge breeder, are focused by means of electrostatic quadrupole doublets and bent by two 180° dipole magnets resulting in a racetrack-like shape. After one revolution the optics realises horizontally and vertically a point-to-point image independent from the charge state of the ions. The second order geometric aberrations as well as most of the chromatic aberrations vanish. The non-zero energy dependant aberrations are compensated by the charge dependant aberrations leading to an effectively achromatic system up to the second order. The beam optical calculations have been carried out with the arbitrary order beam physics code COSY INFINITY and been validated with the beam envelope code TRANSPORT.

Motivation:

Element	q+ Charge	Yield %
^{20}Ne	4	7.5
^{23}Na	6	1.3
^{64}Zn	10	2.8
^{69}Ga	11	2
^{85}Rb	13	5
^{88}Sr	14	3.7
^{109}Ag	17	3
^{115}In	18	3.3
^{120}Sn	19	4.1

Tab.: Efficiency yields obtained for routine operation [2].

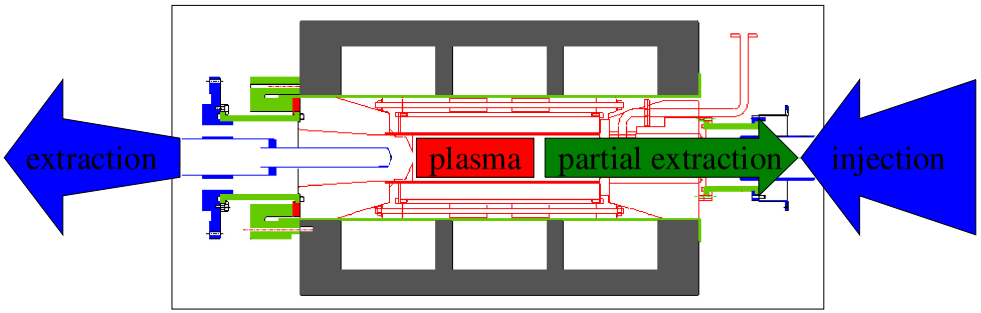

Fig.: The PHOENIX ECRIS charge state booster developed at LPSC Grenoble [3]. **Drawing provided with friendly permission by Th. Lamy.**

Element	1+ Intensity nA
^{20}Ne	1000
^{23}Na	660
^{64}Zn	42
^{69}Ga	460
^{85}Rb	90
^{88}Sr	470
^{109}Ag	175
^{115}In	130
^{120}Sn	167

Idea:

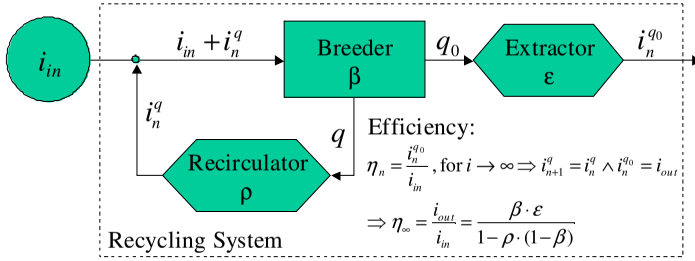

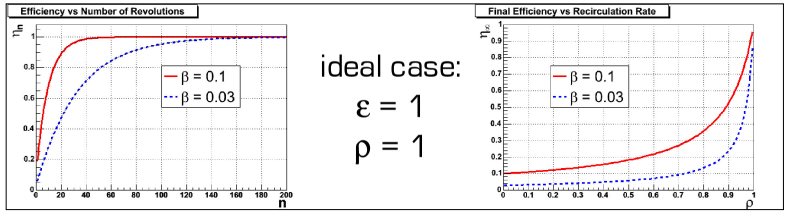

ideal case:
ε = 1
ρ = 1

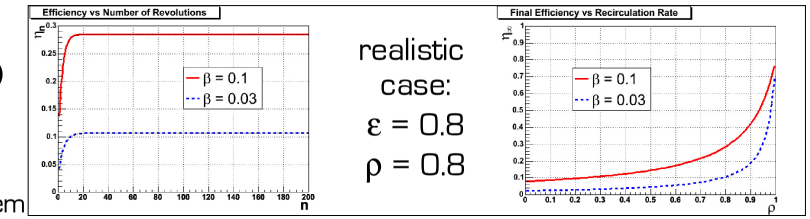

realistic case:
ε = 0.8
ρ = 0.8

$$i_{n+1}^q = (1-\beta)\cdot\rho\cdot(i_{in}+i_n^q) \qquad i_{n+1}^{q_0} = \beta\cdot\varepsilon\cdot(i_{in}+i_{n+1}^q)$$

β: breeding rate of q_0
ε: extraction rate of q_0
ρ: recirculation rate of q
n: number of revolution
q_0: reference (desired) charge state
q: all other charge states
i_{in}: ion current injected into the system
i_{out}: ion current extracted from the equilibrated system

Proposal:

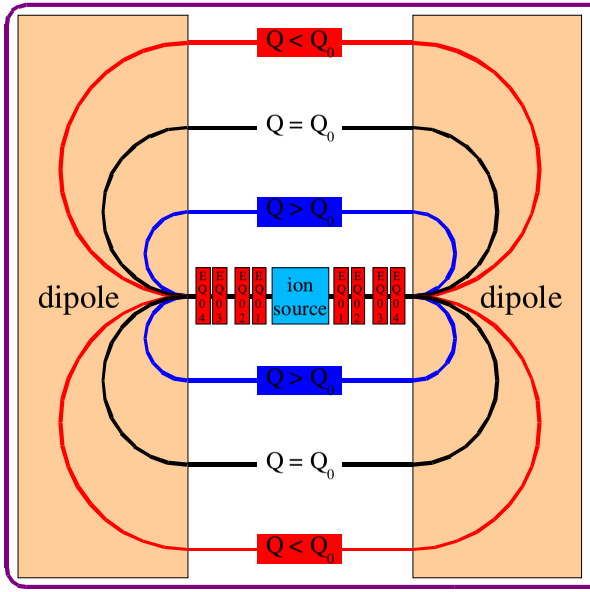

Fig.: Racetrack shaped ion recirculator.
Size: 10×10 m².

Q: arbitrary charge;
Q_0: reference charge;
EQ: electrostatic quadrupoles

Input:

Parameter	Value
Particle	
mass number	A = 140 (e.g. ^{140}Xe)
charge	Q = +20, +1, +40 e
kinetic energy	E_{kin} = 400.0, 20.0, 800.0 keV
electric rigidity	$E\rho$ = 40.0 kV
magnetic rigidity	$B\rho$ = 0.054, 0.241, 0.038 Tm
Beam	
radius	R = 4.0 mm
opening angle	α = ±10.0 mrad
emittance	ε = 40.0 πmm·mrad
current	I = 1.0 mA (only TRANSPORT)

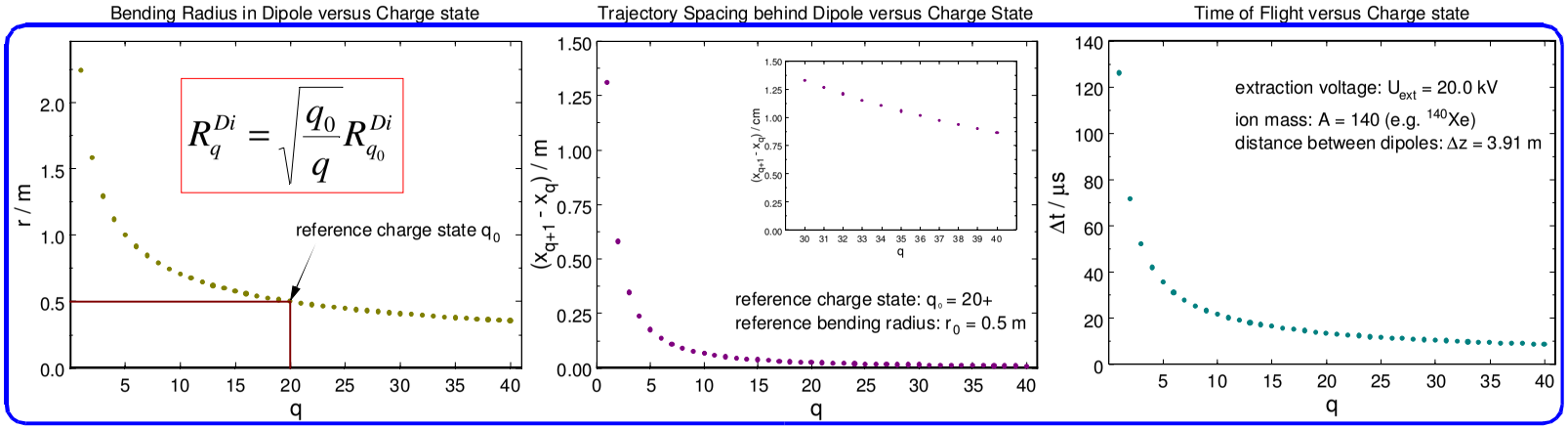

COSY INFINITY Simulations [4]

☑rays; ☑3rd order

Optics 1

Horizontal Plane

q = 1+

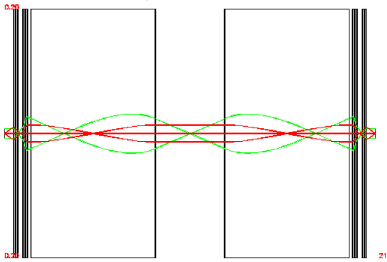

q = 20+

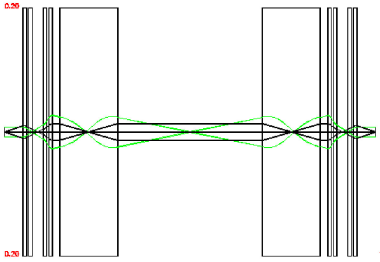

q = 40+

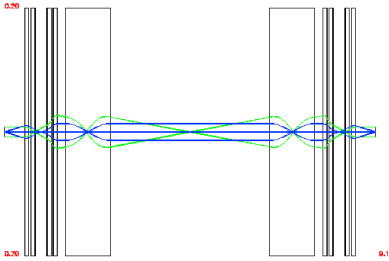

Vertical Plane

q = 1+

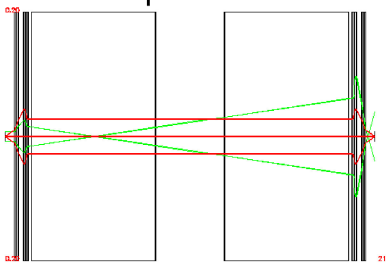

q = 20+

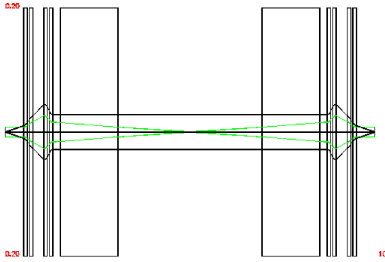

q = 40+

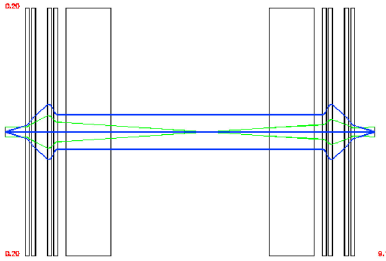

Optics 2

Horizontal Plane

q = 1+

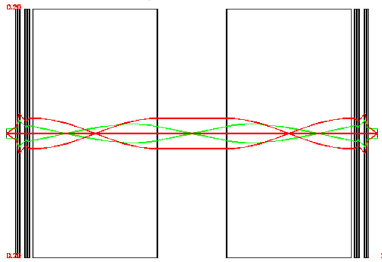

q = 20+

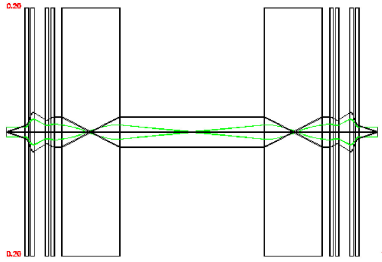

q = 40+

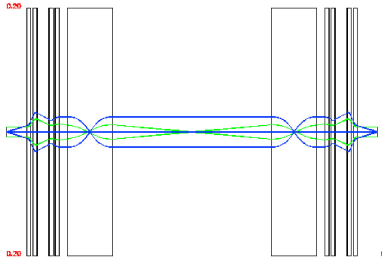

Vertical Plane

q = 1+

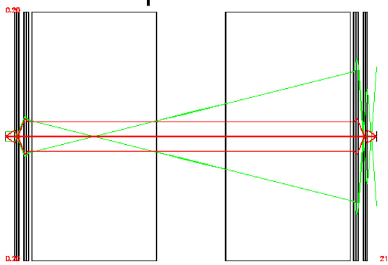

q = 20+

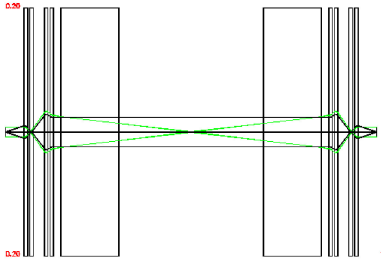

q = 40+

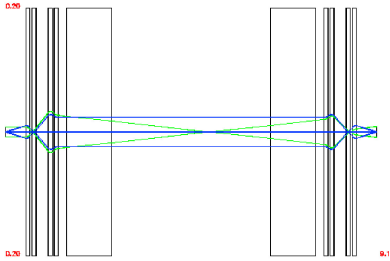

COSY INFINITY Simulations [4]

☑rays; ☑3rd order; ☑fringe fields

Optics 1

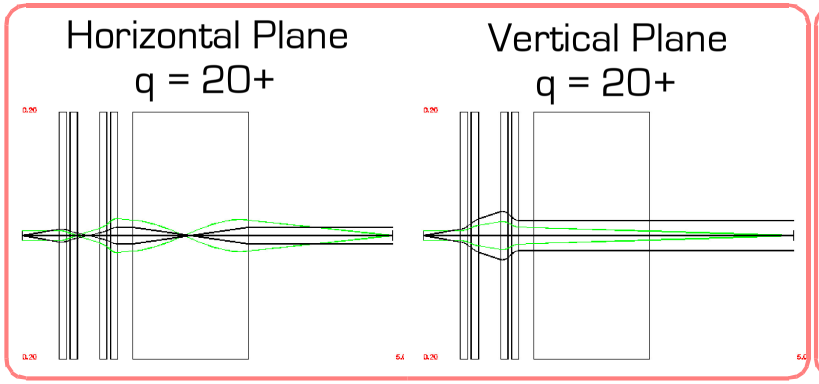

Optics 2

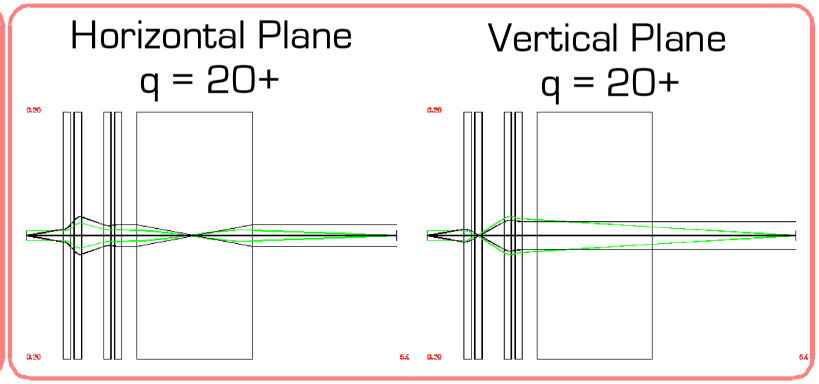

TRANSPORT Simulations [5,6]

☑envelopes; ☑2nd order if ☐space charge; ☑1st order if ☑space charge

Optics 1

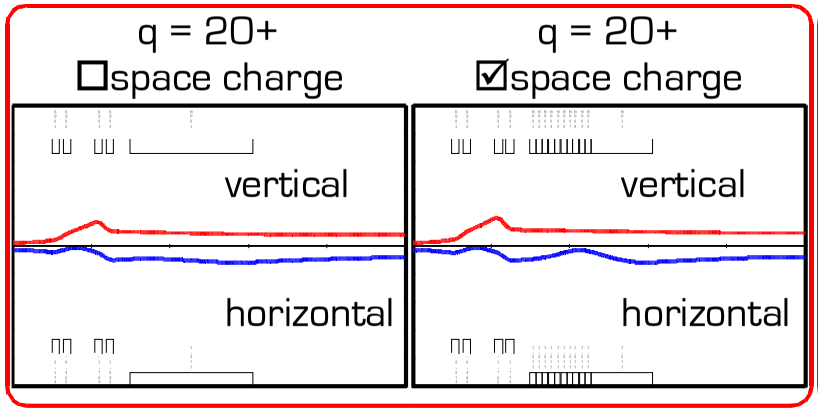

Optics 2

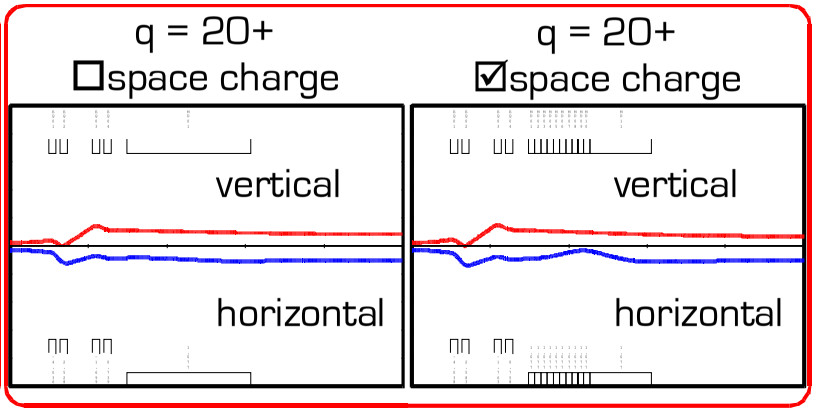

Comparison:

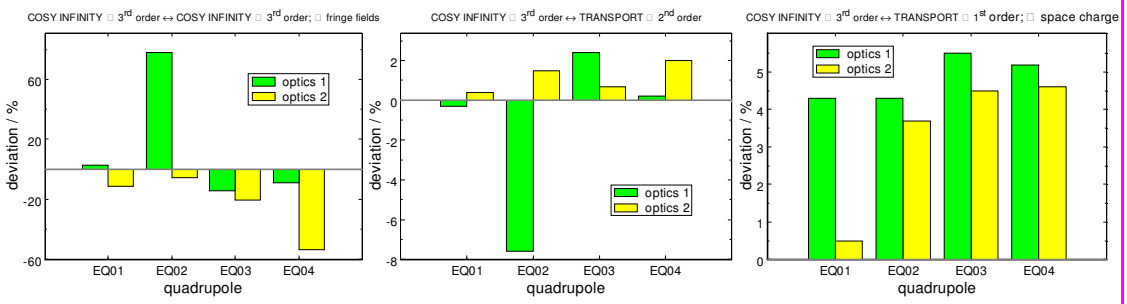

Electro-static Quadru-pole	COSY INFINITY ☑3rd order (reference)		COSY INFINITY ☑3rd order ☑fringe fields		TRANSPORT ☑2nd order		TRANSPORT ☑1st order ☑space charge	
	Optics 1 kV	Optics 2 kV	Optics 1 %	Optics 2 %	Optics 1 %	Optics 2 %	Optics 1 %	Optics 2 %
EQ01	10.9	-20.1	+2.5	-11.2	-0.3	+0.4	+4.3	+0.5
EQ02	-2.3	12.5	+77.9	-5.5	-7.6	+1.5	+4.3	+3.7
EQ03	-8.4	-8.4	-14.4	-20.5	+2.4	+0.7	+5.5	+4.5
EQ04	8.4	3.6	-8.8	-53.4	+0.2	+2.0	+5.2	+4.6

Conclusion:

The beam optics of an ion recirculator for charge breeders consisting of two 180° dipole magnets and eight electrostatic quadrupoles has been investigated with the codes COSY and TRANSPORT. The comparison of the results is resumed in the table on the left. An agreement in the per cent range is observed between COSY and TRANSPORT ($I = 0$ mA). The voltages necessary to focus a space charge beam with $I = 1.0$ mA rest within reasonable limits according to the TRANSPORT simulation. The concept is promising and the work should be continued to arrive at a technical realisation.

References:

[1] *Some Methods of Generation of Multicharged Ions of Radiaoactive and Stable Isotopes*, E.A. Lamzin et al., 6th European Particle Accelerator Conference, Stockholm, Sweden, 22-26 June (1998) 1406-1408.

[2] *Charge Breeding Method Results with the PHOENIX Booster ECR Ion Source*, T. Lamy et al., 8th European Particle Accelerator Conference, Paris, France, 3-7 June (2002) 1724-1726.

[3] *Charge Breeding*, European Commission-RTD Project, Contract HPRI-CT-1999-50003, Final Report, 1 March 2004.

[4] *COSY INFINITY Version 8.1 User's Guide and Reference Manual* M. Berz, MSUHEP-20704, Department of Physics and Astronomy, Michigan State University, 2002.

[5] *TRANSPORT: a computer program for designing charged-particle beam-transport systems; rev. version*, K.L. Brown, D.C. Carey, F.Ch. Iselin, F. Rothacker, CERN Report 80-04, 1980.

[6] PSI Graphic Transport Framework by U. Rohrer based on a CERN-SLAC-FERMILAB version by K.L. Brown et al., December 2003.